Article

Developmental Cell

ZFP281 controls transcriptional and epigenetic changes promoting mouse pluripotent state transitions via DNMT3 and TET1

Graphical abstract

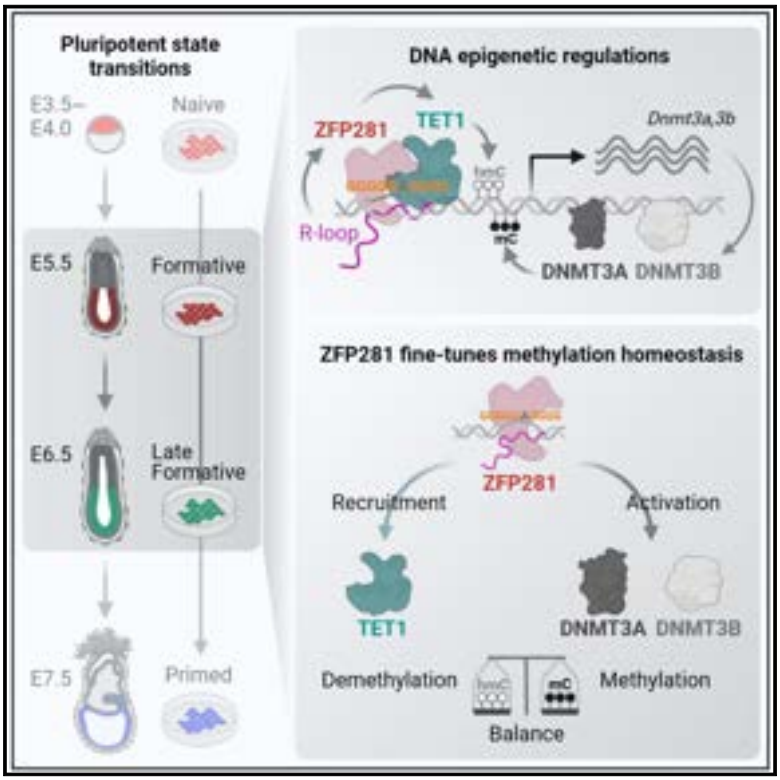

Highlights

- ZFP281 activates *Dnmt3a/3b* in pluripotent stem cells *in vitro* and epiblast *in vivo*
- ZFP281 and TET1 undergo bimodal chromatin occupancy in pluripotent state transitions
- ZFP281 and TET1 chromatin binding depends on the formation of R-loops at promoters
- ZFP281 is necessary for the establishment and maintenance of primed pluripotency

Authors

Xin Huang, Sophie Balmer, Cong Lyu, ..., Anna-Katerina Hadjantonakis, Hongwei Zhou, Jianlong Wang

Correspondence

xh2200@cumc.columbia.edu (X.H.), jw3925@cumc.columbia.edu (J.W.)

In brief

The naive, formative, and primed pluripotent states and their interconversions recapitulate the pluripotency continuum during early development. Huang et al. investigate the transcriptional programs and identify an essential role for ZFP281 in coordinating DNMT3A/3B and TET1 to establish the DNA methylation and gene expression programs during the pluripotent state transitions.

Huang et al., 2024, Developmental Cell *59*, 465–481
February 26, 2024
https://doi.org/10.1016/j.devcel.2023.12.018

CellPress

Developmental Cell

CellPress

Article

ZFP281 controls transcriptional and epigenetic changes promoting mouse pluripotent state transitions via DNMT3 and TET1

Xin Huang,[1,*] Sophie Balmer,[2] Cong Lyu,[3] Yunlong Xiang,[4] Vikas Malik,[1] Hailin Wang,[3] Yu Zhang,[4,5] Bishuang Cai,[6] Wei Xie,[4] Anna-Katerina Hadjantonakis,[2] Hongwei Zhou,[1] and Jianlong Wang[1,7,*]

[1]Department of Medicine, Columbia Center for Human Development and Stem Cell Therapies, Herbert Irving Comprehensive Cancer Center, Columbia University Irving Medical Center, New York, NY 10032, USA

[2]Developmental Biology Program, Sloan Kettering Institute, Memorial Sloan Kettering Cancer Center, New York, NY 10065, USA

[3]Research Center for Eco-Environmental Sciences, Chinese Academy of Sciences, Beijing 100085, China

[4]Tsinghua Center for Life Sciences, School of Life Sciences, Tsinghua University, Beijing 100084, China

[5]Obstetrics and Gynecology Hospital, Institute of Reproduction and Development, Fudan University, Shanghai 200082, China

[6]Division of Liver Diseases, Department of Medicine, Icahn School of Medicine at Mount Sinai, New York, NY 10029, USA

[7]Lead contact

*Correspondence: xh2200@cumc.columbia.edu (X.H.), jw3925@cumc.columbia.edu (J.W.)

https://doi.org/10.1016/j.devcel.2023.12.018

SUMMARY

The progression from naive through formative to primed *in vitro* pluripotent stem cell states recapitulates epiblast development *in vivo* during the peri-implantation period of mouse embryo development. Activation of the *de novo* DNA methyltransferases and reorganization of transcriptional and epigenetic landscapes are key events that occur during these pluripotent state transitions. However, the upstream regulators that coordinate these events are relatively underexplored. Here, using *Zfp281* knockout mouse and degron knockin cell models, we identify the direct transcriptional activation of *Dnmt3a/3b* by ZFP281 in pluripotent stem cells. Chromatin co-occupancy of ZFP281 and DNA hydroxylase TET1, which is dependent on the formation of R-loops in ZFP281-targeted gene promoters, undergoes a "high-low-high" bimodal pattern regulating dynamic DNA methylation and gene expression during the naive-formative-primed transitions. ZFP281 also safeguards DNA methylation in maintaining primed pluripotency. Our study demonstrates a previously unappreciated role for ZFP281 in coordinating DNMT3A/3B and TET1 functions to promote pluripotent state transitions.

INTRODUCTION

Mammalian embryonic development involves DNA methylome remodeling with an initial drastic genome-wide DNA demethylation followed by the re-establishment of the methylation landscape within the pluripotent epiblast during the peri-implantation period.[1,2] Methylation of DNA cytosine to 5-methylcytosine (5mC) is an epigenetic modification associated with transcriptional repression.[3] In mammalian cells, DNA methylation is established by the *de novo* DNA methyltransferases DNMT3A and DNMT3B and maintained by DNMT1 through cell division. Deletion of these enzymes in mice results in embryonic (*Dnmt1* or *Dnmt3b*) or postnatal (*Dnmt3a*) lethality.[4–6] In contrast, DNA demethylation, mediated by the ten-eleven translocation (TET) dioxygenases, oxidizes 5mC to generate 5-hydroxymethylcytosine (5hmC) and its further oxidized species that can eventually be removed to become an unmethylated cytosine.[7] The functional interaction between DNMT3 and TET shapes the mammalian DNA methylome and is essential for early development.[8–10] DNMT3A and DNMT3B are recruited onto gene bodies through histone H3K36me2 and H3K36me3 marks along with gene transcription.[11,12] In contrast, the TET enzymes, which are primarily located at regulatory elements such as gene promoters and enhancers, form DNA hypomethylated valleys.[13–15] However, how the TET enzymes are recruited to the tissue-specific gene regulatory regions remains elusive.[9]

DNA methylation and demethylation dynamics play critical roles in the regulation of gene expression during cell fate commitment and early development coincident with the reorganization of the chromatin occupancy of pluripotency and tissue-specific transcription factors (TFs) for target gene regulation. Pluripotency is a developmental continuum that encompasses a series of successive states,[16] including the naive, formative, and primed states of pluripotency that can be recapitulated by *in vitro* culture of embryonic stem cells (ESCs), epiblast-like cells (EpiLCs), and epiblast stem cells (EpiSCs), respectively.[17] Pluripotency-associated TFs such as OCT4, SOX2, and NANOG are highly expressed in ESCs where they collaboratively inhibit lineage differentiation and preserve an undifferentiated state.[18]

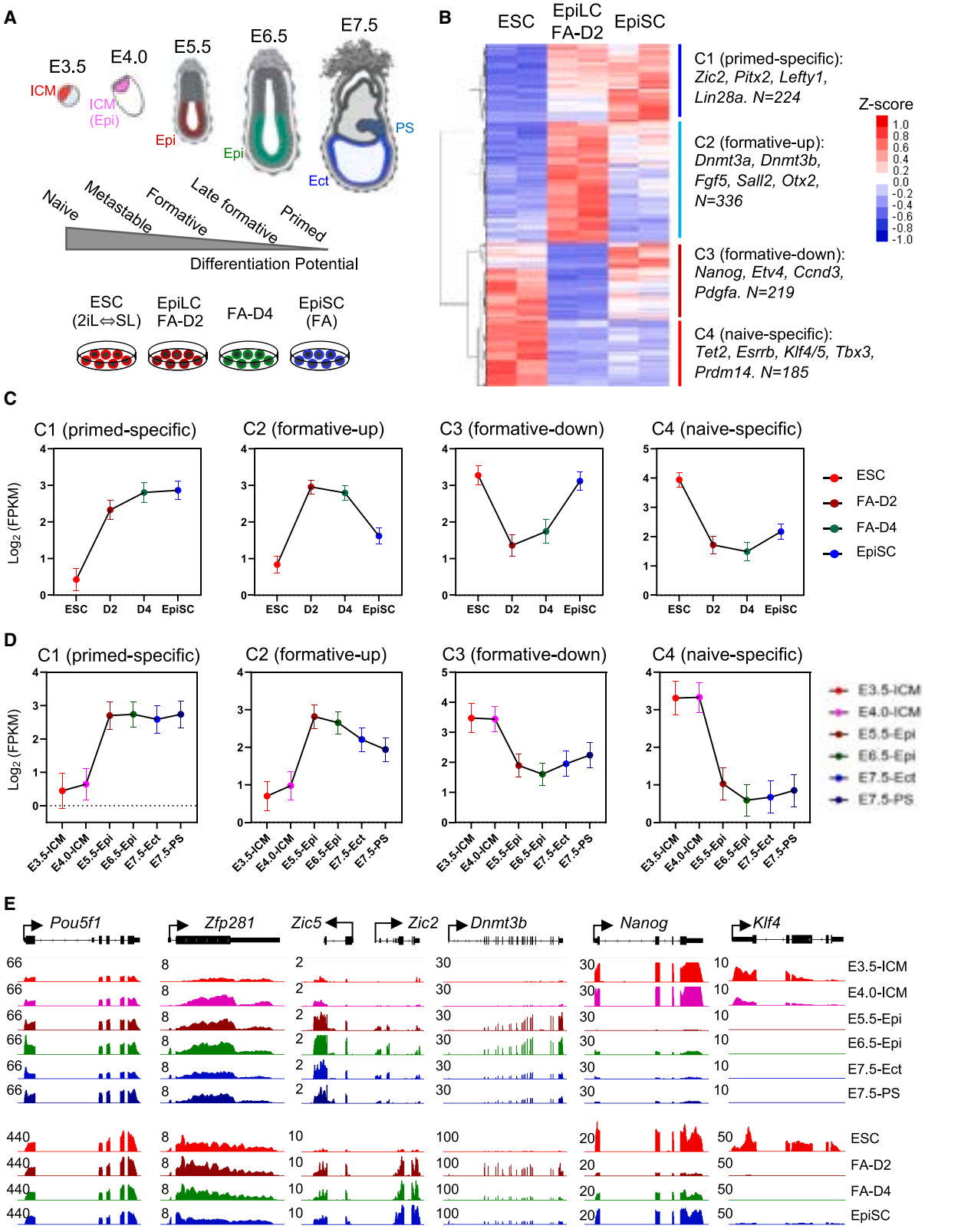

(legend on next page)

Interestingly, while OCT4 and SOX2 are expressed similarly in naive, formative, and primed states, NANOG expression is reduced in the formative state, and its expression follows a biphasic pattern of "on-off-on" during the naive-formative-primed transition *in vitro* and *in vivo*.[19] ZFP281 is a key partner of OCT4 in ESCs and during the naive-to-primed pluripotent state transition, where it functions to reorganize enhancer landscapes.[20–22] We previously reported that ZFP281 coordinates opposing functions of TET1 and TET2 in epigenomic reconfiguration, promoting the naive-to-primed pluripotent state transition *in vitro*,[21] corroborated by its essential and cell-autonomous roles in postimplantation epiblast development *in vivo*.[22,23]

In this study, we further unravel the transcriptional and epigenetic mechanisms underlying the pluripotent state transitions by employing our *Zfp281* knockout (*Zfp281*KO) mouse model[22] and a newly created degron system for rapid ZFP281 protein degradation in pluripotent stem cells (PSCs). We uncovered a previously unknown direct transcriptional control of *Dnmt3a* and *Dnmt3b* by ZFP281 in the early postimplantation embryonic day 6.5 (E6.5) epiblast and in cultured PSCs recapitulating the naive-formative-primed transition and maintenance of primed pluripotency. In addition, we discovered a bimodal pattern of "high-low-high" chromatin occupancy of ZFP281 and TET1, dependent on the formation of R-loops at ZFP281 targeted promoters, and autoregulation of DNMT3A/3B during the pluripotent state transitions.

RESULTS

The transcriptional programs are dynamically regulated in PSCs and during early embryo development

The transition between successive pluripotent states within the epiblast *in vivo* can be recapitulated in *in vitro* cultured PSCs, including naive ESCs cultured in 2 inhibitors and leukemia inhibitory factor (LIF) (2iL),[24] metastable ESCs cultured in serum and LIF (SL), formative EpiLCs by adapting ESCs in Fgf2 and activin culture (FA) for ~2 days, and the primed EpiSCs in the long-term FA culture, as illustrated in Figure 1A (reviewed by Hadjantonakis and colleagues[19]). To understand the dynamic gene transcriptional programs associated with these distinct pluripotent states, we first compared the transcriptomes between ESCs (SL) and formative EpiLCs (FA-D2) and identified 964 differentially expressed genes (DEGs, $p < 0.05$, fold-change > 2; Table S1). As expected for distinct formative and primed pluripotent states, most of them (62.3%, 601/964) were not among the DEGs by comparing ESCs and primed EpiSCs (Figures S1A and S1B). We then performed hierarchical clustering analysis for the 964 formative DEGs and identified four clusters (C1~C4) with distinct expression patterns in ESCs, EpiLCs, and EpiSCs (Figure 1B). The C1 genes are mainly primed state-specific genes (e.g., *Zic2*, *Pitx2*, *Lefty1*, and *Lin28a*) with progressively increased expression in EpiLCs and EpiSCs. In contrast, the C4 genes were mainly naive state-specific genes (e.g., *Tet2*, *Esrrb*, *Klf4/5*, and *Prdm14*) with progressively decreased expression in EpiLCs and EpiSCs. We were particularly interested in the C2 and C3 cluster genes, which were upregulated ("formative-up" genes hereafter, e.g., *Dnmt3a/3b*, *Fgf5*, *Sall2*, and *Otx2*) and downregulated ("formative-down" genes hereafter, e.g., *Nanog*, *Etv4*, *Ccnd3*, and *Pdgfa*) only in the formative state, respectively (Figure 1B). Gene Ontology (GO) analysis of biological processes identified that the C2 genes were involved in the "regulation of transcription, DNA-templated," and "DNA methylation," while the C3 genes are involved in the "cell differentiation," "nervous system development," and "angiogenesis" (Figure S1C). Next, to understand the dynamic transcriptome change during the formative-to-primed transition, we examined an intermediate state between formative and primed states, referred to as the "late formative" state, by adapting ESCs in FA culture for 4 days (FA-D4) (Figure 1A). We plotted the average expression of C1~C4 genes from different pluripotent states of PSCs (Figure 1C) and of corresponding embryonic stages[1] (Figure 1D). Consistently, the formative-up (C2, e.g., *Dnmt3a/3b*) and formative-down (C3, e.g., *Nanog*) genes showed high and low expression levels, respectively, in E5.5–E6.5 epiblasts. Primed-specific genes (C1, e.g., *Zic2/5*) were highly expressed in E7.5 tissues, whereas naive-specific genes (C4, e.g., *Klf4*) were highly expressed in inner cell mass (ICM) of E3.5 and E4.0 embryos (Figures 1C–1E).

In contrast to dynamically expressed genes during pluripotent state transitions, other pluripotency factors, e.g., *Oct4 (Pou5f1)* and *Zfp281* (Figure 1E), were consistently expressed across all pluripotent states. We decided to focus on studying the molecular functions of ZFP281 in these pluripotent states and during the transition for the following reasons. First, we[21] and others[25] have shown that ZFP281 is essential for primed pluripotency, and *Zfp281* epiblast tissue-specific mouse mutants manifested cell-autonomous developmental abnormalities at E6.0 and died E7.75,[22,23] spanning the formative-to-primed transition period *in vitro* (Figure 1A). However, our understanding of the mechanisms underlying this formative-to-primed transition is limited. Second, we have shown that ZFP281 interacts with TET1 and mediates transcriptional and posttranscriptional repression of TET2 in promoting primed pluripotency.[21] We noted here that, similar to ZFP281, TET1 is also expressed across all pluripotent states,[26] whereas TET2 is a "naive-specific" C4 gene that is downregulated in formative and primed states (Figure 1B). TET3 is not expressed across any pluripotent

Figure 1. The dynamic gene expression during the pluripotent state transition

(A) An overview of mouse embryonic development from E3.5 to E7.5, representing the naive, metastable, formative, late formative, and primed pluripotent states. ESCs in serum/LIF (SL) culture were adapted in FGF2 and activin (FA) culture for 2 days (FA-D2) and 4 days (FA-D4) to derive formative (EpiLC) and late formative cells, respectively. Primed EpiSCs were maintained in FA culture. ICM, inner cell mass; Epi, epiblast; Ect, embryonic ectoderm; PS, primitive streak.

(B) Heatmap depicting differentially expressed genes (DEGs) from RNA-seq analysis in ESCs, EpiLCs (FA-D2), and EpiSCs. Four clusters of genes with distinct expression patterns were identified. In each cluster, the total number and a few representative genes were labeled.

(C and D) Average expression by $\log_2$FPKM (fragments per kilobase per million reads) of each gene cluster in different PSCs (C) or embryo lineages (D). Line plots represent the mean expression value with a 95% confidence interval.

(E) RNA-seq tracks (numbers indicate reads per million (RPM) values) depicting expression of pluripotency-related genes in different PSCs or embryo lineages (from our published study[1]).

states. Therefore, TET1 is the only functioning TET enzyme in formative and primed states.[26] How ZFP281 might function with TET1 during the formative-to-primed transition has not been studied. Third, we also noted that *Dnmt3a/3b* are formative-up C2 genes, which are known to be activated by FGF signaling[27] and upregulated in formative PSCs (Figures 1B and 1E, bottom), as well as in E5.5–E6.5 postimplantation embryos (Figure 1E, top). However, despite the well-recognized roles of DNA methylation in embryonic development,[1,5,28] how DNMT genes are transcriptionally activated in early embryos remains poorly understood. We thus decided to explore ZFP281 as a candidate factor regulating DNMT gene expression to fill this knowledge gap.

De novo DNA methyltransferases are regulated by ZFP281 in postimplantation embryos

We first examined whether the DNMT genes are directly regulated by ZFP281 in the epiblast of developing embryos. From our RNA-seq analysis of wild-type (WT) and *Zfp281*$^{-/-}$ E6.5 embryos,[22] we found that mRNA expression levels of the DNMT3 family genes *Dnmt3a*, *3b*, and *3l*, but not *Dnmt1*, are reduced in mutant embryos compared with WT embryos (Figure S2A). We also performed shRNA-mediated knockdown of *Zfp281* in ESCs and EpiSCs and found that sh*Zfp281* reduced the expression of *Dnmt3a*, *3b*, and *3l* genes, but not *Dnmt1* (Figure S2B), consistent with the *in vivo* results (Figure S2A). To assess the defects in *Zfp281* mutant embryos at the protein level, we performed single-cell quantitative immunofluorescence (qIF)[29] and found that DNMT3A, 3B, and 3L proteins were significantly reduced in the *Zfp281*$^{-/-}$ E6.5 epiblast compared with those in WT epiblast (Figures 2A–2D). To examine whether DNA methylation is affected in the epiblast of *Zfp281* mutants, we applied small-scale TELP-enabled methylome sequencing (STEM-seq[1]) for low-input genome-wide DNA methylome profiling of WT, *Zfp281*$^{+/-}$, and *Zfp281*$^{-/-}$ E6.5 embryos. We found that DNA methylation at CG (mCG) sites decreased in the *Zfp281*$^{+/-}$ embryos and further still in the *Zfp281*$^{-/-}$ embryos relative to WT embryos at E6.5 (Figure 2E).

Reanalysis of our published chromatin immunoprecipitation followed by deep sequencing (ChIP-seq) data[22] and ChIP-qPCR of ZFP281 in ESCs and EpiSCs identified that ZFP281 directly binds to the regulatory elements at *Dnmt3a*, *3b*, and *3l* loci (Figures S2C and S2D). Interestingly, the ESC and EpiSC ZFP281 binding peaks on *Dnmt3a* and *Dnmt3b* loci coincided with regions of DNA hypomethylation in postimplantation embryonic tissues (Figure 2F). Altogether, our results suggest that ZFP281 may transcriptionally activate *Dnmt3a/3b/3l* by direct binding at their regulatory loci (i.e., promoters) with DNA hypomethylation valleys during postimplantation development.

ZFP281 directly activates DNMT3A/3B expression in controlling the transcription programs of formative and late formative pluripotent states

To address whether ZFP281 chromatin binding facilitates *Dnmt3a/3b* promoter demethylation during the peri-implantation embryonic development, we employed the *in vitro* pluripotent state transition model as a scalable alternative to the limited availability of embryonic tissues at these stages. Because the loss of *Zfp281* affects the self-renewal of primed EpiSCs but not ESCs,[21] we established a degron[30] cell system for rapid, inducible, and reversible ZFP281 protein degradation in ESCs (Figure 3A, two independent clones, #2 and #21, see details in STAR Methods). Although ZFP281 expression level in the degron cells was slightly lower than that in the parental WT cells even before the dTAG treatment (Figure S3A), we excluded the possibility of spontaneous degradation in degron cells, manifested by the preserved lower expression of ZFP281 in degron cells than WT cells under proteasome inhibitor MG132 treatment (Figure S3B). Using *Zfp281*^{degron} ESCs, we confirmed that dTAG could induce near-complete protein degradation within 2 h (Figure 3A). Importantly, ZFP281 depletion by dTAG also decreased DNMT3A and DNMT3B expression in ESCs, whereas the removal of dTAG reintroduced their protein expression (Figure S3C). Of note, the *Dnmt3a* gene is transcribed from two alternative promoters (Figure 2F), resulting in two transcript isoforms: the long isoform *Dnmt3a1* and the short isoform *Dnmt3a2*, respectively.[13,31] The *Dnmt3b* gene also has multiple splice variants, but the *Dnmt3b* isoforms share the same promoter and have similar protein sizes (Figure S2C). In ESCs, DNMT3A2 is predominantly expressed, while DNMT3A1 and DNMT3B isoforms are lowly expressed (Figure S3D). Without dTAG, *Zfp281*^{degron} ESCs could be adapted in FA culture to derive EpiSCs, referred to as converted EpiSCs (cEpiSCs, Figure S3D). ZFP281 is steadily expressed in all pluripotent states, with a slightly higher expression in ESCs and FA-D2 cells than in FA-D4 cells and cEpiSCs (Figures 3B and S3D). In contrast, *Zfp281*^{degron} ESCs could not be maintained in the FA culture for more than 3 passages in the presence of dTAG, consistent with our finding using *Zfp281*KO ESCs.[21] We also examined ZFP281 function in the formative FA-D2 and late formative FA-D4 samples and found that depletion of ZFP281 by dTAG diminished the activation of DNMT3A and DNMT3B and delayed the reduction of naive-specific markers (e.g., KLF4 and ESRRB) at both protein (Figures 3B and S3E) and RNA (Figure S3F) levels. More importantly, the global levels of DNA 5mC were decreased in FA-D2 (orange bars) and FA-D4 (light green bars) cells upon dTAG treatment measured by mass spectrometry quantification (Figure 3C) and DNA dot blot analysis of genomic DNA (Figure S3G). We also observed that DNA 5hmC was increased in the presence of dTAG (Figures 3C and S3G), likely due to the loss of DNMT3A/3B activity, leading to increased TET1 activity and DNA 5hmC.[13]

To understand how ZFP281 depletion affects gene transcription programs in distinct pluripotent states, we performed RNA-seq analysis of *Zfp281*^{degron} ESCs, FA-D2, and FA-D4 cells in the presence or absence of dTAG and compared them with embryo-derived WT ESCs and EpiSCs (Figure 3D). Principal-component analysis (PCA) for the WT and *Zfp281*^{degron} samples without dTAG treatment demonstrated a trajectory of classic naive ESCs toward the formative/late formative and primed states (Figure 3E). However, with dTAG, *Zfp281*^{degron} FA-D2 and FA-D4 samples deviated from the transition. In addition, the dTAG-treated FA-D4 samples are far away from the untreated FA-D4 samples but relatively closer to the FA-D2 samples (Figure 3E, dashed circle), indicating a major defect in the formative-to-late formative transition upon ZFP281 depletion. We examined the expression levels of C1∼C4 genes (Figure 1B) in *Zfp281*^{degron} RNA-seq data and found that ZFP281 depletion

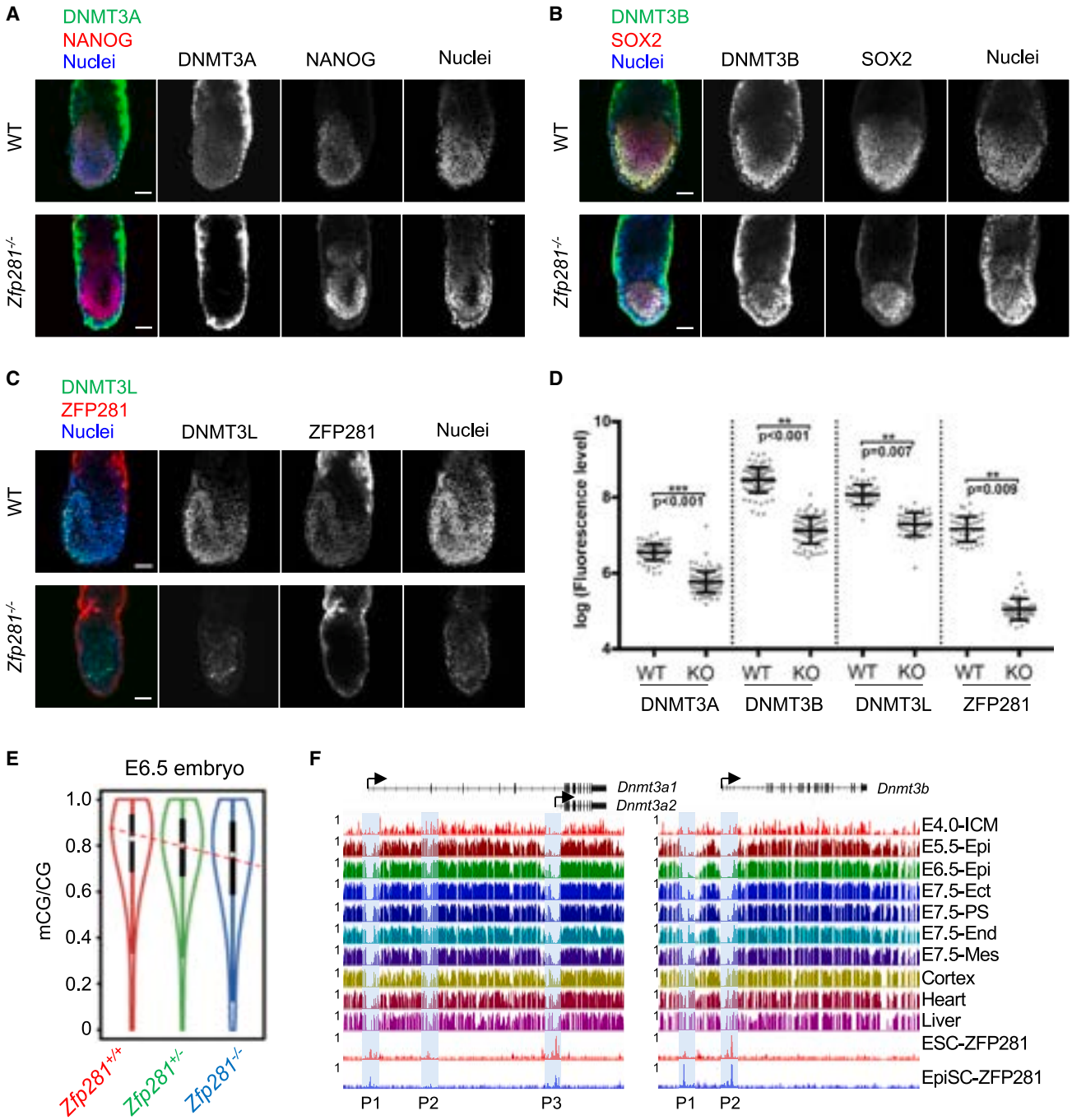

Figure 2. *De novo* DNA methyltransferases are regulated by ZFP281 in postimplantation embryos

(A–C) Immunostaining of DNMT3A and NANOG (A), DNMT3B and SOX2 (B), and DNMT3L and ZFP281 (C) in WT and *Zfp281*$^{-/-}$ embryos (E6.5). The NANOG, SOX2, and ZFP281 are used as references for nuclear staining. In each genotype, at least 3 embryos were used for staining (n = 3).

(D) Fluorescent intensity of ZFP281 and DNMT3 family proteins was quantified using Imaris software. Each dot represents the mean corrected fluorescence level per epiblast cell. p value is from a two-tailed t test.

(E) The CG methylation (mCG) levels in the WT, *Zfp281*$^{+/-}$, and *Zfp281*$^{-/-}$ E6.5 embryos.

(F) DNA-methylation landscapes (numbers indicate mCG values) in postimplantation embryonic lineages (E4.0–E7.5) and three adult tissues (from our published study[1]) and ZFP281 ChIP-seq tracks in ESCs and EpiSCs at *Dnmt3a* and *Dnmt3b* loci. The ZFP281 ChIP peaks (P1–P3) were labeled.

compromised the activation of the C1 genes (primed-specific, e.g., *Zic2* and *Pitx2*) and delayed the reduction of the C4 (naive-specific, e.g., *Klf4* and *Tet2*) genes (Figures 3F and 3G). ZFP281 depletion also decreased the expression of the C2 genes (formative-up, e.g., *Dnmt3a*, *Dnmt3b*) and increased the C3 genes (formative-down, e.g., *Nanog*, *Pdgfa*) in FA-D2 and

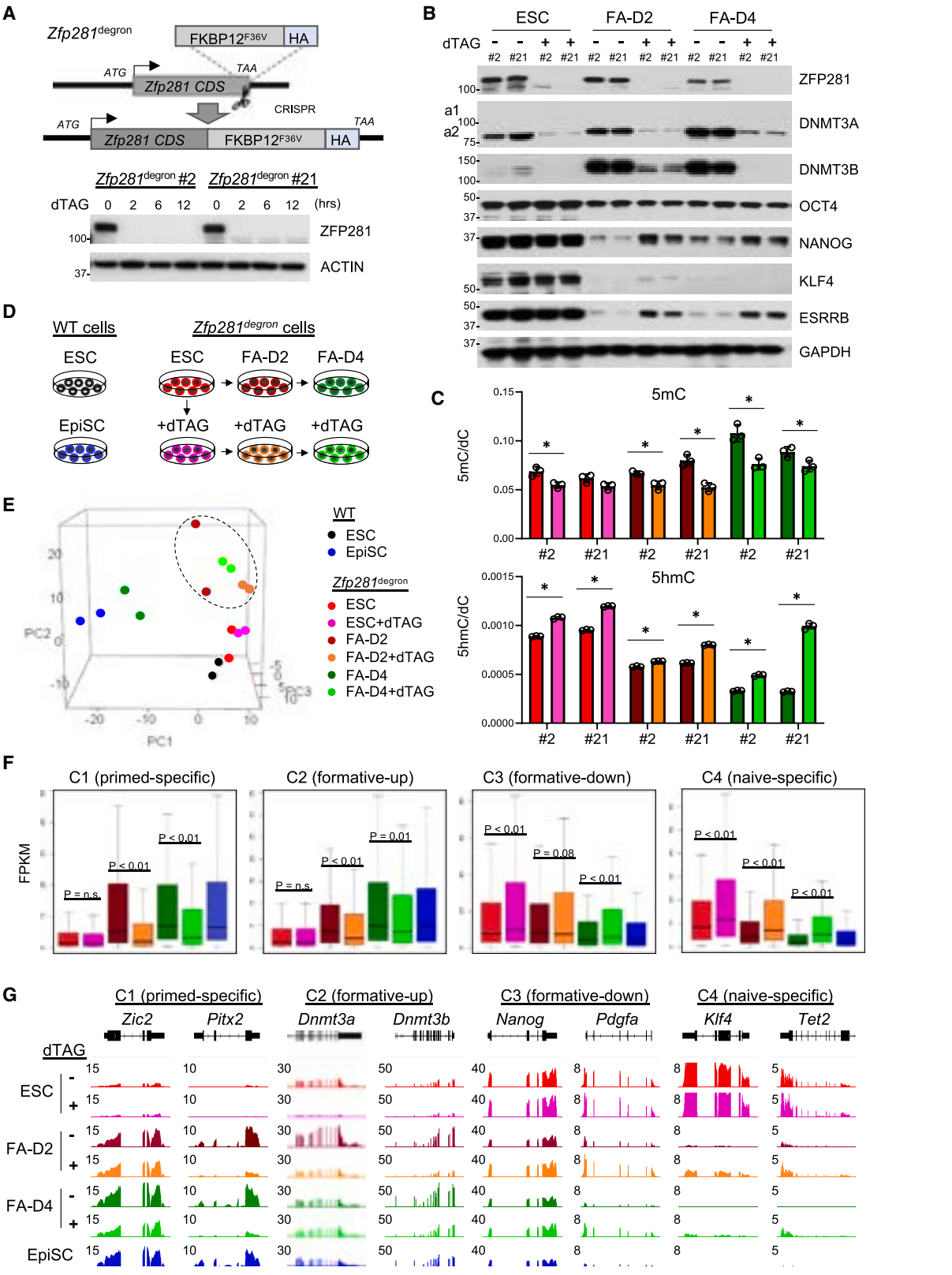

(legend on next page)

FA-D4 samples (Figures 3F and 3G). Thus, our results suggest that ZFP281 is an important TF assisting the switch of transcriptional programs during the pluripotent state transitions.

The *de novo* DNA methylation established by DNMT3A/3B must be maintained by DNMT1 through cell division. Although DNMT1 is present within the epiblast at E6.5 and in PSCs, it is not regulated by ZFP281 (Figures S2A and S2B). To address whether the DNMTs are critical in the naive-to-primed pluripotent state transition, we employed WT, *Dnmt1*-KO, *Dnmt3a/3b*-DKO, and *Dnmt1/3a/3b*-TKO ESCs and performed ESC-to-EpiSC differentiation. We were able to convert *Dnmt1*-KO and *Dnmt3a/3b*-DKO ESCs to cEpiSCs, which is consistent with the finding that *Dnmt3a/3b* single or double KO mice appeared to develop normally until E8.5.[5,28] However, we failed to convert *Dnmt1/3a/3b*-TKO ESCs to cEpiSCs (Figures S3H and S3I), consistent with the G2/M cell cycle arrest and enhanced cell death during epiblast differentiation of these TKO cells.[32] The apparent discrepancy in the establishment of the primed pluripotent state between *Zfp281*KO[21] and *Dnmt3a/3b*-DKO ESCs could be due to the engagement of additional key factors downstream of ZFP281 in this state transition[25] (see discussion).

Dynamic chromatin occupancy of ZFP281/TET1 and feedback control of DNMT3A/3B in the pluripotent state transitions

Given that activation of DNMT3 family genes depends on the transcriptional activity of ZFP281 and that ZFP281 can recruit TET1 for targeted DNA demethylation at certain loci,[21] we asked how ZFP281 might coordinate both classes of DNA epigenetic regulators to regulate downstream target genes during the pluripotent state transitions. We performed ChIP-seq analysis of ZFP281 by antibody pull-down in WT ESCs, FA-D2, FA-D4 cells, and EpiSCs and by HA-tag pull-down in *Zfp281*^{degron} ESCs, FA-D2, and FA-D4 cells (no dTAG, as a biological replicate; Figure 4A). The ChIP-seq data obtained from the two pull-downs showed a good correlation at different pluripotent states (Figure S4A), demonstrating the high quality of the dataset. First, we compared the ZFP281 peaks identified in WT ESCs and EpiSCs and observed a genome-wide rearrangement of chromatin-bound ZFP281 (Figure 4B). Motif analysis for the ESC-only, EpiSC-only, and ESC/EpiSC-shared peaks of ZFP281 identified a consensus G-rich motif (Figures 4C and S4B), suggesting ZFP281 actively binds to its target loci in respective pluripotent states. When plotting the ZFP281 ChIP intensity at all its peak regions (N = 12,732), we were surprised to note that the average intensity in the FA-D2 samples was significantly lower than that of the other states (Figure 4D). Next, we performed TET1 ChIP-seq in the same cell states (Figure 4A). Interestingly, we observed low TET1 ChIP intensity at the ZFP281 peaks in the FA-D2 samples (Figure 4E). However, such a trend was not observed by plotting TET1 ChIP intensity at all transcription start sites (TSSs) (Figure S4C), reinforcing the ZFP281-dependent recruitment of TET1 at the ZFP281 target sites. By plotting the ZFP281 and TET1 ChIP intensity at the ZFP281 peaks that are individually called in each state, we obtained a similar result (Figures S4D–S4F) as we observed at the 12,732 ZFP281 peaks (Figures 4D and 4E), suggesting that chromatin-bound ZFP281 decreased globally and that there is no redistribution of ZFP281 during the naive-to-formative transition. When comparing the ZFP281 peak intensity between different pluripotent states, we found that the intensity of most peaks was decreased (N = 3,804) in the ESC-to-FA-D2 transition but was increased (N = 1,695) in the FA-D2-to-FA-D4 transition (Figure 4F), highlighting a major regulatory event happening during the naive-formative-late formative transition. We then compared the 3,084 and 1,695 significantly altered ZFP281 peaks and found that many of the same peaks (N = 945) decreased in ESC-to-FA-D2 transition and then recovered in FA-D2-to-FA-D4 transition (Figure 4G). GO analysis for the target genes of 945 ZFP281 peaks (TSS < 5,000 bp) identified that they were involved in the "regulation of cell cycle," "multicellular organism development," "chromatin organization," and "cell differentiation" (Figure S4G). Together, our data suggest that chromatin-bound ZFP281 and TET1 at a subgroup of ZFP281 peaks exhibited a bimodal high-low-high occupancy pattern during the naive-formative-late formative transition, which was maintained high thereafter till the primed EpiSC state (Figure 4I). A regained chromatin occupancy of ZFP281 and TET1 in the late formative state is likely a key epigenetic event via DNA hypomethylation to reactivate those ZFP281 target genes that are downregulated in the formative state (Figures 1B and 4H, the C3 genes).

Next, we asked whether other pluripotency-associated TFs or epigenetic regulators are dynamically distributed along with ZFP281 during pluripotent state transitions. Previously we showed that ZFP281 interacts with the pluripotency TF OCT4 and histone acetyltransferases P300/P400 in ESCs and EpiSCs.[21,22] From a published dataset of ESC-to-FA-D2 transition,[20] we found that ChIP intensity of OCT4 and P300 were decreased along with ZFP281 (at 3,804 ZFP281 peaks with

Figure 3. ZFP281 activates DNMT3A and DNMT3B in the pluripotent state transitions

(A) Schematic depiction of the *Zfp281*^{degron} knockin strategy. The HA-tagged FKBP12^{F36V} donor sequence was inserted at the end (TAA) of *Zfp281* coding sequence (CDS) to create an in-frame fusion protein. Two *Zfp281*^{degron} ESC clones (#2 and #21) were derived. ZFP281 protein was depleted within 2 h upon treatment of dTAG.

(B) Western blot analysis for *Zfp281*^{degron} ESCs, FA-D2, and FA-D4 cells. DNMT3A2 (a2) is the predominant isoform, and DNMT3A1 (a1) is faint in regular exposure. Another blot containing both DNMT3A isoforms by long exposure is shown in Figure S3E.

(C) UHPLC-MS/MS quantification for 5mC (top) and 5hmC (bottom) intensity in the genomic DNA of *Zfp281*^{degron} PSCs with or without dTAG treatment. An intensity ratio of 5mC or 5hmC over deoxycytidine (dC) was measured. Experiments were performed in technical triplicates (n = 3); p value is from a two-tailed t test, and *p < 0.05.

(D) Schematic depiction of the pluripotent state transitions using *Zfp281*^{degron} PSCs. WT ESCs and EpiSCs were used as the reference states. *Zfp281*^{degron} ESCs were treated with dTAG for 2 days, and then both untreated and treated ESCs were adapted to FA culture condition without (top) or with (bottom) dTAG treatment.

(E) Principal-component analysis (PCA) depicting RNA-seq samples of WT and *Zfp281*^{degron} PSCs.

(F and G) Boxplots of C1∼C4 cluster genes (F) and RNA-seq tracks (numbers indicate RPM values) of representative genes (G) depicting their expression in *Zfp281*^{degron} PSCs during pluripotent state transitions. p value is from a paired Mann-Whitney test, "n.s." denotes statistically non-significant.

(A–G) Two *Zfp281*^{degron} clones (#2 and #21, as biological replicates) were used. All color codes refer to (D).

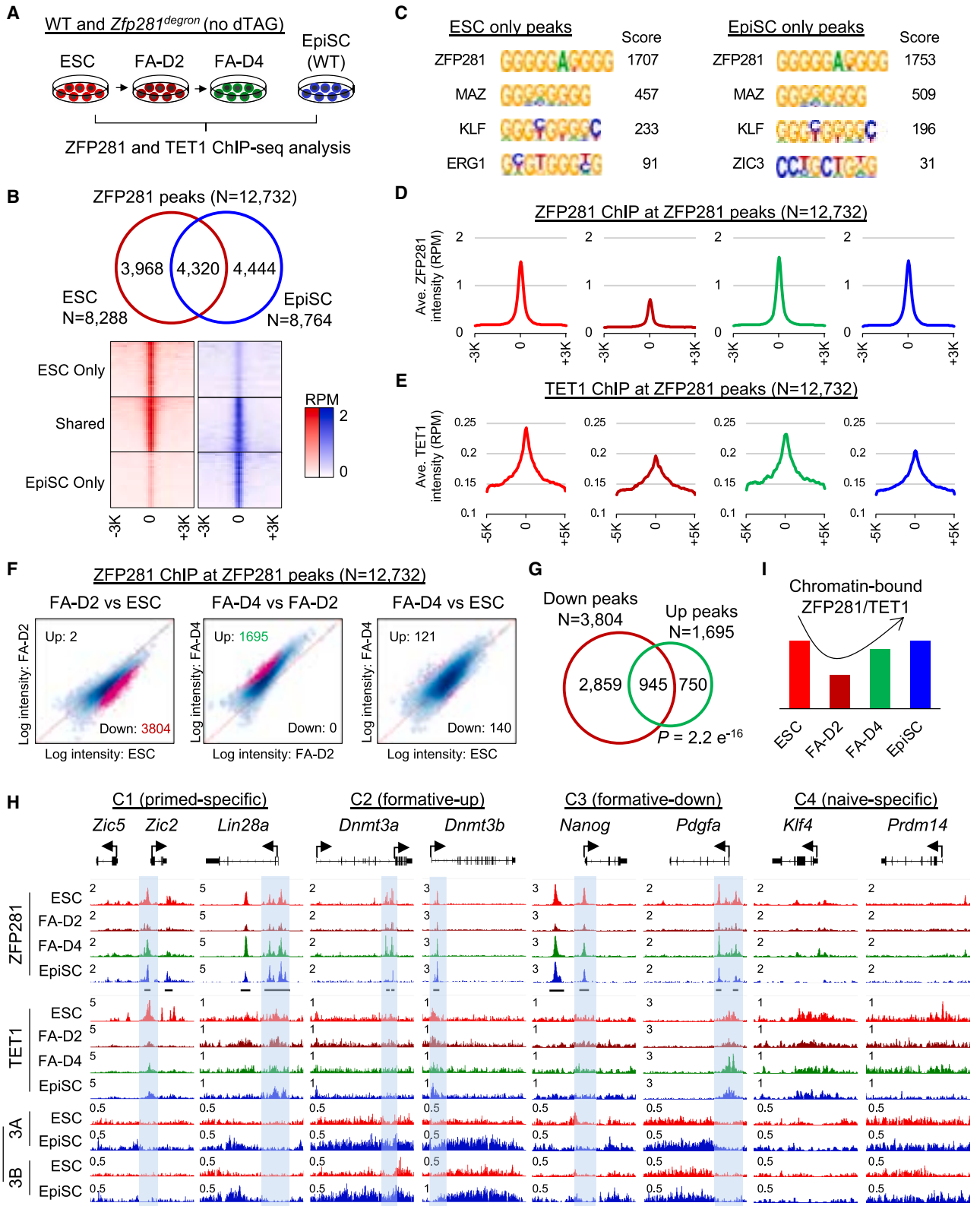

(legend on next page)

decreased intensity) (Figure S4H). From another published dataset of a 3-day EpiSC-to-ESC reprogramming,[33] we observed a similar pattern, although in a reverse direction of pluripotent state transition. OCT4 and NANOG showed decreased ChIP intensity from day 0 to day 1, and then increased intensity at days 2 and 3 at the ZFP281 peaks, as well as at all the identified OCT4 or NANOG peaks (Figures S4I and S4J). Together, these data support our finding that ZFP281, as a component of a transcriptional complex containing OCT4 and P300 with consistent expression levels in different pluripotent states (Figures 1E and 3B), follows a bimodal pattern of chromatin occupancy with high-low-high binding intensity during the naive-formative-primed transitions.

Because DNMT3A and DNMT3B are highly activated in the primed state (Figure S3D), we also performed DNMT3A/3B ChIP-seq in WT EpiSCs and compared the data with the ChIP-seq data in ESCs.[34] We found that DNMT3A/3B mainly bind across gene bodies to deposit DNA 5mC modification in ESCs and EpiSCs (Figure S4K, "all genes"), while hypomethylation status at promoters was protected by TET1 and additional factors (i.e., ZFP281) in ESCs and EpiSCs, as well as during the pluripotent state transitions (Figure 4H, gene promoters with ZFP281 peaks in C1∼C3). Interestingly, when examining the DNMT3A and DNMT3B ChIP intensity across gene bodies of C1∼C4 cluster genes associated with the state transitions (Figure 1B), we found that only C1/C2 but not C3/C4 genes displayed higher DNMT3A/3B-binding intensity in EpiSCs than ESCs (Figure S4K), likely because C1/C2 genes are transcriptionally activated during the naive-to-primed transition (Figure 1B) and that DNMT3A/3B bind to gene bodies that undergo active transcription.[12,34] Because *Dnmt3a* and *Dnmt3b* are among the C2 genes, our data also suggest a transcriptional autoregulation of *Dnmt3a* and *Dnmt3b* (Figure 4H), downstream of their activation by ZFP281, during pluripotent state transitions.

ZFP281 harnesses TET1 chromatin association in the naive-to-formative state transition

We further investigated the ZFP281-dependent TET1 chromatin association during the pluripotent state transition. Using the *Zfp281*^{degron} ESCs, we performed the naive-to-formative transition with and without dTAG treatment and TET1 ChIP-seq analysis (Figure 5A). First, we confirmed that dTAG treatment significantly reduced ZFP281 ChIP signal in ESCs (Figure S5A). Importantly, ZFP281 depletion by dTAG reduced TET1 ChIP intensity at all TET1 peaks (N = 9,764, Figure 5B) and at all TSSs in ESCs (Figure S5B). However, TET1 ChIP intensity was increased in EpiLCs by dTAG treatment (Figures 5B and S5B), likely due to compromised DNMT3A/3B activity that leads to an increased distribution of TET1 in EpiLCs. Next, we compared the TET1 peak intensity between untreated ESCs and EpiLCs, and in ESCs and EpiSCs with or without dTAG treatment. We identified 1,922 and 629 TET1 peaks with significantly higher and lower intensity, respectively, in EpiLCs than ESCs (Figure 5C). The intensity of most TET1 peaks was decreased (N = 501) upon dTAG treatment in ESCs; however, fewer peaks were increased (N = 85) by dTAG in EpiLCs (Figure 5C). We also compared TET1 intensity at ZFP281 peaks (N = 13,400, determined by comparing the ZFP281 ChIP-seq in untreated vs. dTAG-treated ESCs). Similarly, there were more peaks with decreased TET1 intensity by dTAG treatment in ESCs than those with increased intensity in EpiLCs (227 vs. 70, Figures S5C and S5D). We overlapped these significantly changed TET1 peaks and found a significant overlap (N = 386) between the ESC-to-EpiLC down peaks (N = 629) and ESC + dTAG down peaks (N = 501) (Figure 5D). Altogether, our data support an active TET1 recruitment by ZFP281 in ESCs and during the naive-to-formative state transition.

We further characterized the 386 ESC-to-EpiLC and ESC+-dTAG common down TET1 peaks and found that 162 peaks (42%) were directly targeted by ZFP281 in ESCs (Figure 5E). We also located the target genes of 386 peaks and found that many of these genes (N = 223, TSS < 5,000 bp) were among the C1 (primed-specific) and C2 (formative-up) clusters (Figure 5F). Indeed, GO analysis for these genes identified that they were involved in "multicellular organism development," "neuron differentiation," and "stem cell differentiation" (Figure 5G). We confirmed that chromatin-bound TET1 at promoters decreased upon ZFP281 depletion in ESCs and during the ESC-to-EpiLC differentiation (Figure 5H). We also performed methylated DNA immunoprecipitation (meDIP) analysis and found that both DNA 5mC and 5hmC at promoters were decreased upon ZFP281 depletion in ESCs (Figure S5E), likely due to the decreased DNMT3 activity and impaired TET1 recruitment, respectively. In addition, RNA-seq data indicated that ZFP281 is required to activate the C1/C2 genes during the naive-to-formative transition (Figures 3G and S5F). Considering that chromatin-bound ZFP281 is also decreased in this transition (Figures 4D and 4H), we reasoned that decreased ZFP281 and TET1 at promoters may be important to reduce the repressive effect by Polycomb repressive complex 2 (PRC2) on lineage-specific genes (Figure 5H), as we reported that TET1 can also

Figure 4. Dynamic chromatin occupancy of ZFP281/TET1 and feedback transcriptional control of DNMT3A/3B in the pluripotent state transitions

(A) Schematic depiction of the ZFP281 and TET1 ChIP-seq analysis. HA ChIP in *Zfp281*^{degron} (no dTAG) PSCs was performed as a biological replicate of ZFP281 ChIP in WT PSCs (n = 2). All TET1 ChIP was performed in WT PSCs.

(B) Overlap of the identified ZFP281 peaks (top) and intensity heatmap (bottom) from ZFP281 ChIP-seq analysis in WT ESCs and EpiSCs.

(C) The top enriched motifs identified from the ESC-only and EpiSC-only ZFP281 peaks.

(D and E) Mean intensity plots depicting ZFP281 (D) and TET1 (E) ChIP-seq intensity at ZFP281 peaks.

(F) Scatterplots depicting the distribution of ZFP281 peak intensity by comparing FA-D2 with ESC (left), FA-D4 vs. FA-D2 (middle), and FA-D4 vs. ESC (right) data. Peaks with significantly different intensity is determined by $p < 0.05$.

(G) Overlap of the significantly decreased ZFP281 peaks (N = 3,804) by comparing FA-D2 vs. ESC data and significantly increased peaks (N = 1,695) by comparing FA-D4 vs. FA-D2 data. p value is from a Fisher's extract test.

(H) ChIP-seq tracks (numbers indicate RPM values) depicting the intensity of ZFP281, TET1, DNMT3A, and DNMT3B at representative C1∼C4 genes in different PSCs. The identified ZFP281 peaks are labeled on the bottom of the ZFP281 tracks. The shadows indicate the promoters with a bimodal ZFP281 binding pattern.

(I) Schematic depiction of chromatin-bound ZFP281 and TET1 during pluripotent state transitions.

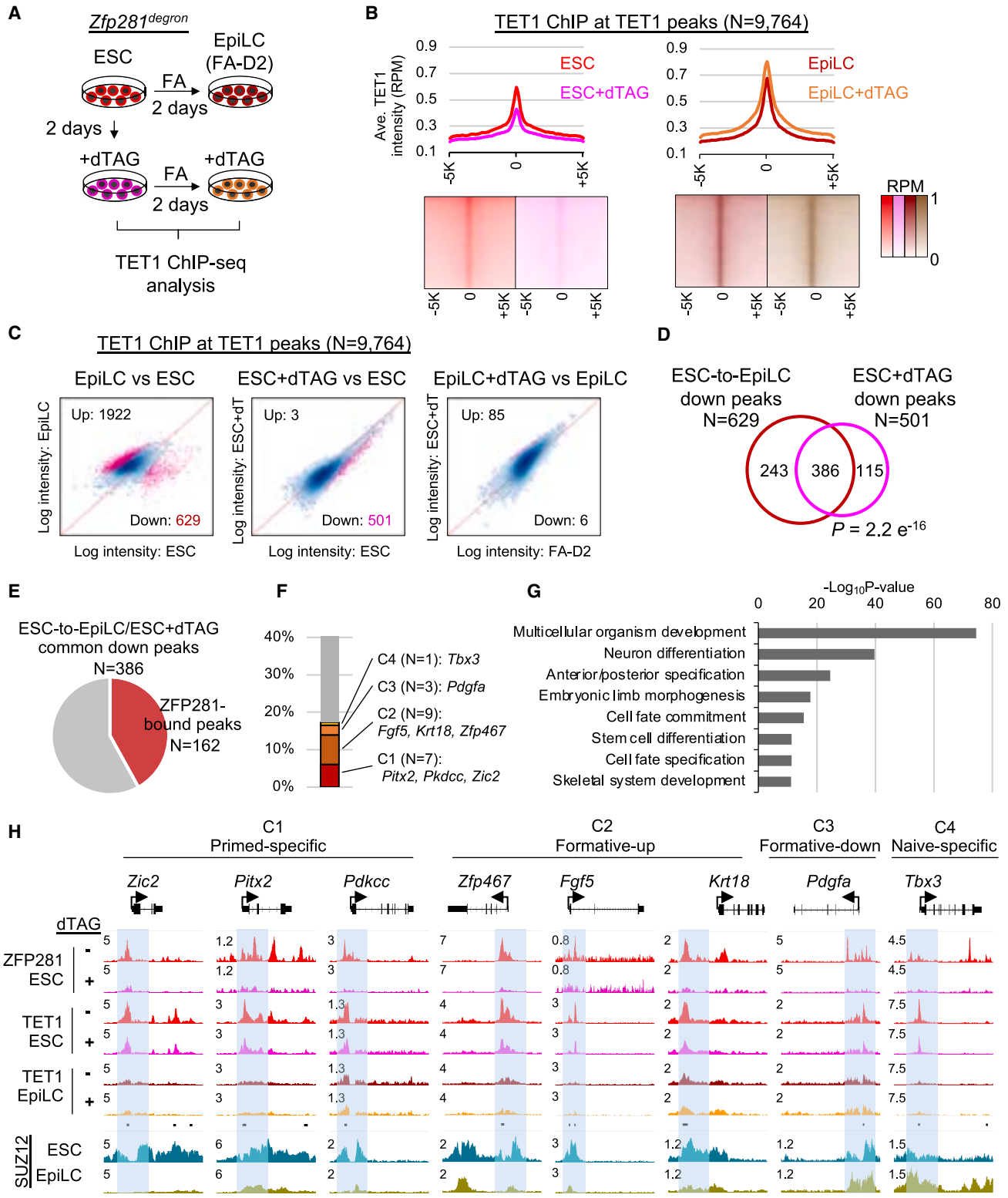

Figure 5. ZFP281 harnesses TET1 chromatin association in the naive-to-formative state transition

(A) Schematic depiction of the *Zfp281*^{degron} ESCs and EpiLCs with dTAG treatment and TET1 ChIP-seq analysis with biological replicates (n = 2).

(B) Mean intensity plots (top) and intensity heatmaps (bottom) depicting TET1 ChIP-seq intensity at TET1 peak regions (±5,000 bp) in untreated and dTAG-treated *Zfp281*^{degron} ESCs and EpiLCs.

(legend continued on next page)

repress the lineage genes through PRC2 during ESC differentiation.[35] However, it was still puzzling that a few C3/C4 genes (Figure 5F, e.g., *Pdgfa* and *Tbx3*) were also bound by ZFP281 and TET1, but their expression was repressed by ZFP281 (Figures 3G and S5F). Regulation of these genes may be independent of PRC2 (Figure 5H) and possibly by reduced DNMT3A/3B expression upon ZFP281 depletion.

ZFP281 safeguards the homeostasis of DNA methylation and demethylation in maintaining primed pluripotency

Having established the critical roles of ZFP281 in coordinating DNMT3 and TET1 functions during the naive-formative-primed pluripotent state transitions, we investigated the mechanism by which ZFP281 maintains primed pluripotency. We took advantage of the *Zfp281*^{degron} cEpiSCs (Figure S3D) and treated them with dTAG for 2 days and 4 days, followed by RNA-seq analysis (Figure 6A). *Zfp281*^{degron} cEpiSCs could not be maintained for 3 passages with persistent dTAG treatment. There were more DEGs identified at day 4 than day 2 of dTAG treatment (comparing day 4 vs. day 0 and day 2 vs. day 0) but with a consistent trend of transcriptome change at the two time points (Figures S6A and S6B), suggesting that transcriptional changes upon ZFP281 depletion are enhanced with a more prolonged dTAG treatment. We performed hierarchical clustering analysis and identified the up- and downregulated DEGs upon ZFP281 depletion in cEpiSCs (Figure 6A; Table S2). Genes associated with lineage development (e.g., *Lefty1*, *Lefty2*, and *Lin28a*), *de novo* DNA methylation (i.e., *Dnmt3a/3b*), WNT signaling pathway and downstream targets (e.g., *Wnt3*, *Wnt8a*, *Lrp5*, *Nkd1*, *Nkd2*, *Ccnd1*, and *Ccnd2*), and somatic differentiation (e.g., HOX cluster genes) were downregulated upon ZFP281 depletion (Figures 6A–6C). In contrast, most naive pluripotency genes (e.g., *Esrrb*, *Zfp42*, *Tet2*, *Klf2*, *Klf4*, and *Prdm14*), DNA demethylation enzymes *Tet1/Tet2*, and factors that are important for primed pluripotency (e.g., *Fgf5*, *Otx2*, and *Zic3*) were upregulated upon ZFP281 depletion (Figures 6A–6C). These results indicate that ZFP281 depletion in cEpiSCs disrupts the primed pluripotency gene expression programs.

To gain a global view of the transcriptional changes, we performed gene set enrichment analysis (GSEA) and GO analysis for the RNA-seq data. These analyses identified that the WNT signaling pathway and DNA methylation/demethylation are among the most significantly perturbed upon ZFP281 depletion (Figures 6D and S6C). Consistently, 5mC and 5hmC levels measured by DNA dot blot (Figure S6D) and quantified by mass spectrometry (Figure S6E) were decreased and increased, respectively, upon ZFP281 depletion, likely due to decreased DNMT3A/3B and increased TET1/2 expression levels in cEpiSCs (Figures 6A–6C).

We also performed PCA for the RNA-seq data, showing that the transcriptome of day 2 + dTAG *Zfp281*^{degron} cEpiSCs was closer to that of WT and *Zfp281*^{degron} ESCs with or without dTAG (Figure 6E, dashed circle). However, extended dTAG treatment caused the transcriptome of day 4 + dTAG *Zfp281*^{degron} cEpiSCs (Figure 6E, purple dots) to deviate away from any other states. These data suggest that cEpiSCs with ZFP281 depletion were first reverted to an ESC-like state before deregulating further into an undefined state. Furthermore, when examining the expression of C1∼C4 cluster genes in the *Zfp281*^{degron} cEpiSCs with dTAG treatment (day 0, day 2, and day 4), we found that ZFP281 depletion decreased the expression of C1 genes and increased the C4 genes (Figure 6F). However, expression of C2/C3 genes was not affected by ZFP281 depletion, suggesting that ZFP281's transcriptional regulation of C2/C3 genes is critical for the ESC-EpiLC-EpiSC transition but dispensable for EpiSC self-renewal/maintenance (Figures 3F and 6F). Together, these results demonstrate that, although ZFP281 regulates distinct transcription programs for the maintenance vs. establishment of primed pluripotency, the regulation of DNA methylation/demethylation homeostasis is likely a conserved function of ZFP281 essential for both these processes.

ZFP281 chromatin association depends on the formation of R-loops

We further explored the mechanism underlying the dynamic ZFP281 chromatin association during the pluripotent state transitions. We showed that ZFP281 mainly binds to DNA with a high G-rich motif (Figures 4C and S4B). It is well established that active transcription on the G-rich (GC skew) DNA template strands is prone to R-loop formation.[36] Interestingly, R-loops are also associated with promoters occupied by TET1 bearing 5hmC modification in ESCs[37] and protect DNA from *de novo* methylation.[36] Therefore, we investigated the relationship between ZFP281/TET1 chromatin binding and the formation of R-loops at ZFP281 targeted promoters.

We used MapR assay to profile genome-wide R-loop distribution during the pluripotent state transitions (Figure 7A). MapR is a modified CUT&RUN-based method that uses a catalytically inactive RNASEH1, which is fused to micrococcal nuclease (MNase) and specifically recognizes (but not digests) R-loops.[39] A MNase-only CUT&RUN is used as a parallel control. From a publicly available MapR dataset in ESCs,[40] we identified that ZFP281 target genes had higher R-loop intensity at promoters than the non-target genes in different expression groups (Figure S7A). Next, we profiled R-loops in different pluripotent states and compared the R-loop intensity at all TSSs (Figure 7A). Interestingly, the overall R-loop intensity was higher in the ESC, FA-D2, and FA-D4 states than in the primed cEpiSC and EpiSC states

(C) Scatterplots depicting the distribution of TET1 peak intensity by comparing (untreated) EpiLC vs. ESC (left), ESC + dTAG vs. ESC (middle), and EpiLC + dTAG vs. EpiLC (right) data. Peaks with significantly different intensity is determined by $p < 0.05$.
(D) Overlap of the significantly decreased TET1 peaks (N = 386) by comparing EpiLC vs. ESC and ESC+dTAG vs. ESC data. p value is from a Fisher's extract test.
(E) Pie chart depicting the number of ZFP281-bound peaks among the 386 common down peaks.
(F) Percentages and representative genes in the C1∼C4 gene clusters among the TET1 target genes (N = 223, TSS < 5,000 bp) identified from the 386 common down peaks.
(G) Gene Ontology (GO) analysis for the 223 TET1 target genes.
(H) ChIP-seq tracks (numbers indicate RPM values) depicting the intensity of ZFP281, TET1, and PRC2 component SUZ12 (from our published study[35]) at representative C1∼C4 genes. TET1 common down peaks are labeled on the bottom of TET1 tracks, and shadows indicate TET1-dependent promoters.

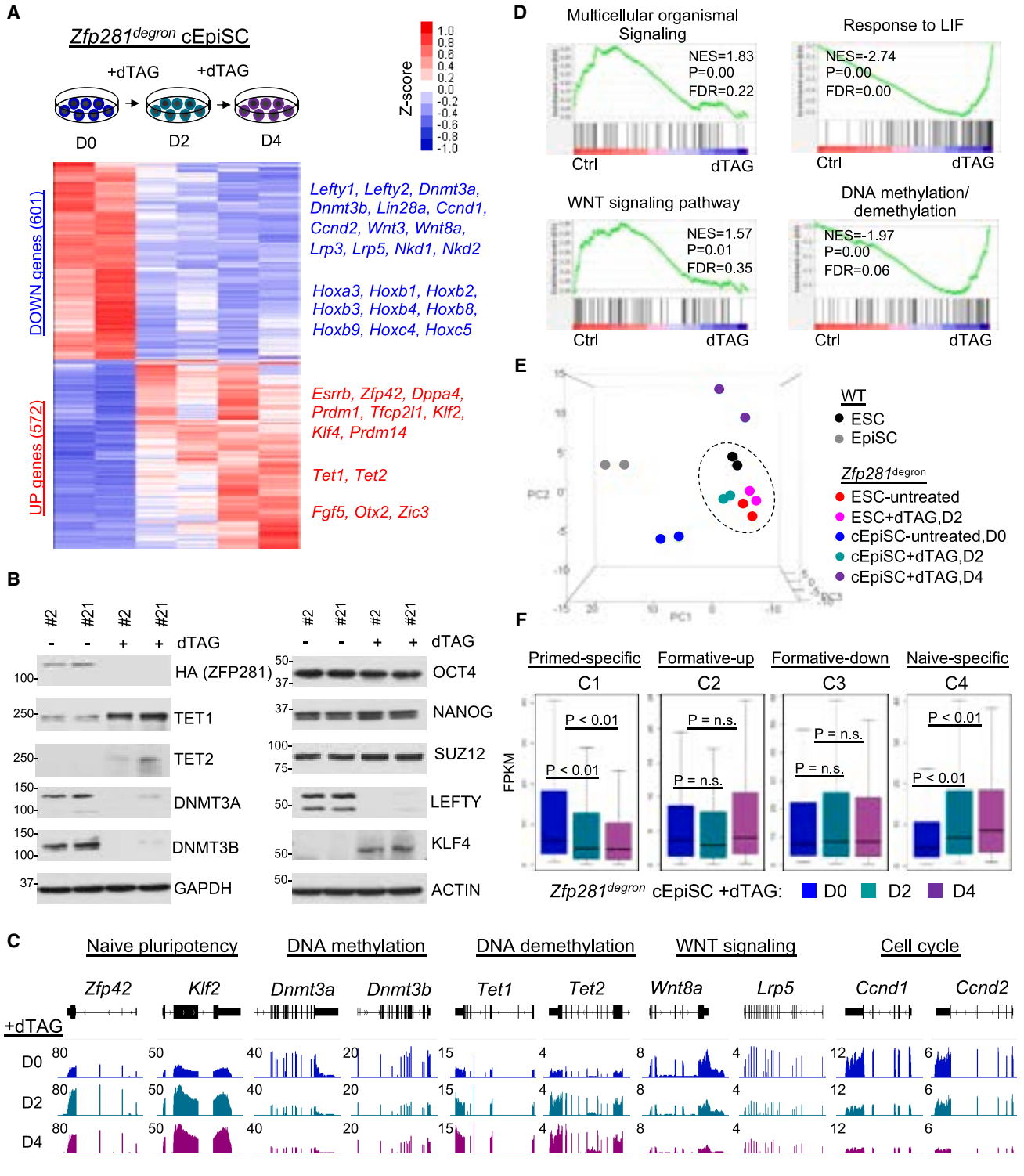

Figure 6. ZFP281 safeguards the homeostasis of DNA methylation and demethylation in maintaining primed pluripotency

(A) Heatmap depicting DEGs from RNA-seq analysis (with two *Zfp281*^{degron} clones, as biological replicates) in *Zfp281*^{degron} cEpiSCs before (day 0) and after dTAG treatment for 2 and 4 days. Representative up- and downregulated genes were shown on the right side of the heatmap.

(B) Western blot analysis for *Zfp281*^{degron} cEpiSCs with dTAG treatment (4 days).

(C) RNA-seq tracks (numbers indicate RPM values) depicting expression of genes in *Zfp281*^{degron} cEpiSCs with dTAG treatment. Genes in different functional groups were labeled.

(legend continued on next page)

(Figure 7A). We examined the R-loop intensity at ZFP281 peaks identified during the pluripotent state transitions (N = 12,732, Figure 4B). Although R-loops intensity at all three groups of ZFP281 peaks reduced during the naive-to-primed transition, R-loops were still enriched at the EpiSC-associated ZFP281 peaks (EpiSC-only and ESC/EpiSC-shared) in the primed cEpiSC and EpiSC states (Figure 7B). To correlate R-loops and associated gene expression, we further examined the R-loop intensity at promoters of the C1∼C4 genes. The C3/C4 (i.e., formative-down/naive-specific) genes are highly expressed in ESCs (Figures 1B and 1C), and consistently, R-loop intensity at their promoters was higher than that of C1/C2 genes (i.e., primed-specific/formative-up) in ESC and FA-D2 states (Figures S7B and S7C). Therefore, our data indicate that C3/C4 genes tend to show R-loop dynamics (i.e., stepwise decreasing) at promoters during pluripotent state transitions (examples given in Figure 7C). In contrast, R-loops at the promoters of lineage genes (i.e., C1/C2 genes) are relatively stable regardless of their expression levels in different pluripotent states (Figures 7C and S7C).

Finally, we asked whether ZFP281 binding at chromatin depends on the formation of R-loops. To this end, we performed ZFP281 ChIP-seq analysis in ESCs with either empty vector (EV) or *Rnaseh1* overexpression (Figure 7D). First, we confirmed that *Rnaseh1* overexpression reduced R-loop levels without disturbing the pluripotency in ESCs (Figures S7D–S7F). Because TET1 can be recruited to chromatin by ZFP281, we also processed published TET1 ChIP-seq data with the same treatment of *Rnaseh1* overexpression in ESCs.[38] Interestingly, both ZFP281 and TET1 ChIP intensity decreased at the ZFP281 peak regions upon *Rnaseh1* overexpression (Figures 7D, 7E, and S7G), suggesting that chromatin association of ZFP281 and TET1 depends on the formation of R-loops. GO analysis for the R-loop-sensitive ZFP281/TET1 target genes (N = 766, TSS < 5,000 bp) identified that they were involved in "regulation of transcription, DNA-templated", "chromatin organization", and "multicellular organism development" (Figure S7H). The R-loop-sensitive ZFP281 and TET1 target genes encompass all 4 cluster genes, and examples for a few C1∼C3 genes are given (Figure S7G). Considering that these genes undergo dynamic expression changes (Figure 1) during pluripotent state transitions and that R-loop intensity is relatively high in the naive, formative, and late formative states (Figures 7A–7C), our data suggest a potential R-loop-dependent positive feedback regulation for gene activation at the GC-skewed ZFP281-bound promoters by TET1 recruitment and DNA demethylation during the pluripotent state transitions.

DISCUSSION

Pluripotency is highly dynamic and is under tight transcriptional and epigenetic control, with gene activation and repression generally corresponding to DNA demethylation and methylation in the context of different states of pluripotency. Studies of the gene expression programs of naive and metastable ESCs, formative EpiLCs, primed EpiSCs, and their interconversions have enriched our molecular understanding of pluripotency progression and cellular reprogramming.[17,20,33,41,42] In this study, we established a central role of ZFP281 in dynamically regulating gene expression via the coordination of DNMT3 and TET1 functions in pluripotent state transitions. We identified 4 groups of genes, whose expression is differentially regulated during the naive-to-formative-to-primed cell state transitions coordinated with a distinct bimodal pattern of ZFP281 and TET1 chromatin occupancy, a decrease of R-loop formation, and an increase of DNA methylation (Figure 7F). Moreover, we identified an FA-D4 late formative state of pluripotency (Figure 7F) where the ZFP281/TET1 chromatin binding patterns are similar to the primed state (Figures 4D and 4E), the R-loop levels are similar to the naive and formative states (Figures 7A–7C), and the gene expression profiles are closer to the formative state (Figure 1C). The relatively narrow bimodal ZFP281/TET1 chromatin occupancy pattern (Figure 7F) supports that chromatin reorganization by TFs and epigenetic regulators precedes the gene expression changes during the pluripotent state transitions. Our results also support that naive ESCs, but not primed EpiSCs, rely on high R-loop accumulations at promoters to maintain the transcription activity.[37] Detailed molecular characterization and functional studies using *Zfp281*KO mouse embryos and *Zfp281*^{degron} PSCs establish a complex interplay among ZFP281, TET1, and DNMT3A/3B (Figure 7G). First, ZFP281 and TET1 form a partnership to co-occupy at GC-skewed ZFP281-bound promoters (Figures 4D, 4E, and 5A–5E) and transcriptionally activate them, including *Dnmt3a/3b* genes (Figures 2A–2D, 3B, S2A, S2B, S3C, and S3F). Second, DNMT3A/3B transcriptionally autoregulate their own genes (Figures 4H and S4K). Third, DNMT3A/3B and TET1 functionally antagonize each other in 5mC/5hmC modifications (Figures 3C, S3G, S6D, and S6E), likely due to their physical competition in chromatin occupancy as reported in ESCs.[13] Our study deepens our understanding of the transcriptional and epigenetic mechanisms underlying pluripotent state transitions and early development.

Naive ESCs maintained under 2i and LIF culture exhibit genome-wide hypomethylation and an open chromatin landscape. However, hypomethylation in naive ESCs also leads to eroded genomic imprints and chromosomal abnormalities.[43,44] In contrast, metastable ESCs are constrained from differentiation by SL with considerable expression levels of *Dnmt3a/3b/3l* and *Tet1/2* genes to preserve genomic stability[27] and are thus functionally naive. Using SL ESCs as a starting point for pluripotent state transitions, we demonstrate that ZFP281 transcriptionally activates DNMT3A/3B in different pluripotent states. However, the fact that we could establish primed cEpiSCs from *Dnmt3a/3b*-DKO ESCs (Figure S3I), but not *Zfp281*KO[21] ESCs, suggests that additional transcriptional or epigenetic regulators downstream of ZFP281 are necessary for the establishment of primed pluripotency. Indeed, the histone H3 lysine 9 (H3K9)

(D) Gene set enrichment analysis (GSEA) for the enriched ontology gene sets by comparing the WT EpiSCs and untreated *Zfp281*^{degron} cEpiSCs (Ctrl) vs. the dTAG-treated (2 and 4 days) *Zfp281*^{degron} cEpiSCs. Normalized enrichment score (NES), p value, and false discovery rate (FDR) for the enrichment were indicated with the enrichment plot.

(E) Principal-component analysis (PCA) depicting RNA-seq samples of WT and *Zfp281*^{degron} ESCs and cEpiSCs with dTAG treatment.

(F) Boxplots depicting the expression of C1∼C4 genes in *Zfp281*^{degron} cEpiSCs with dTAG treatment. p value is from a Mann-Whitney test, and "n.s." denotes statistically non-significant.

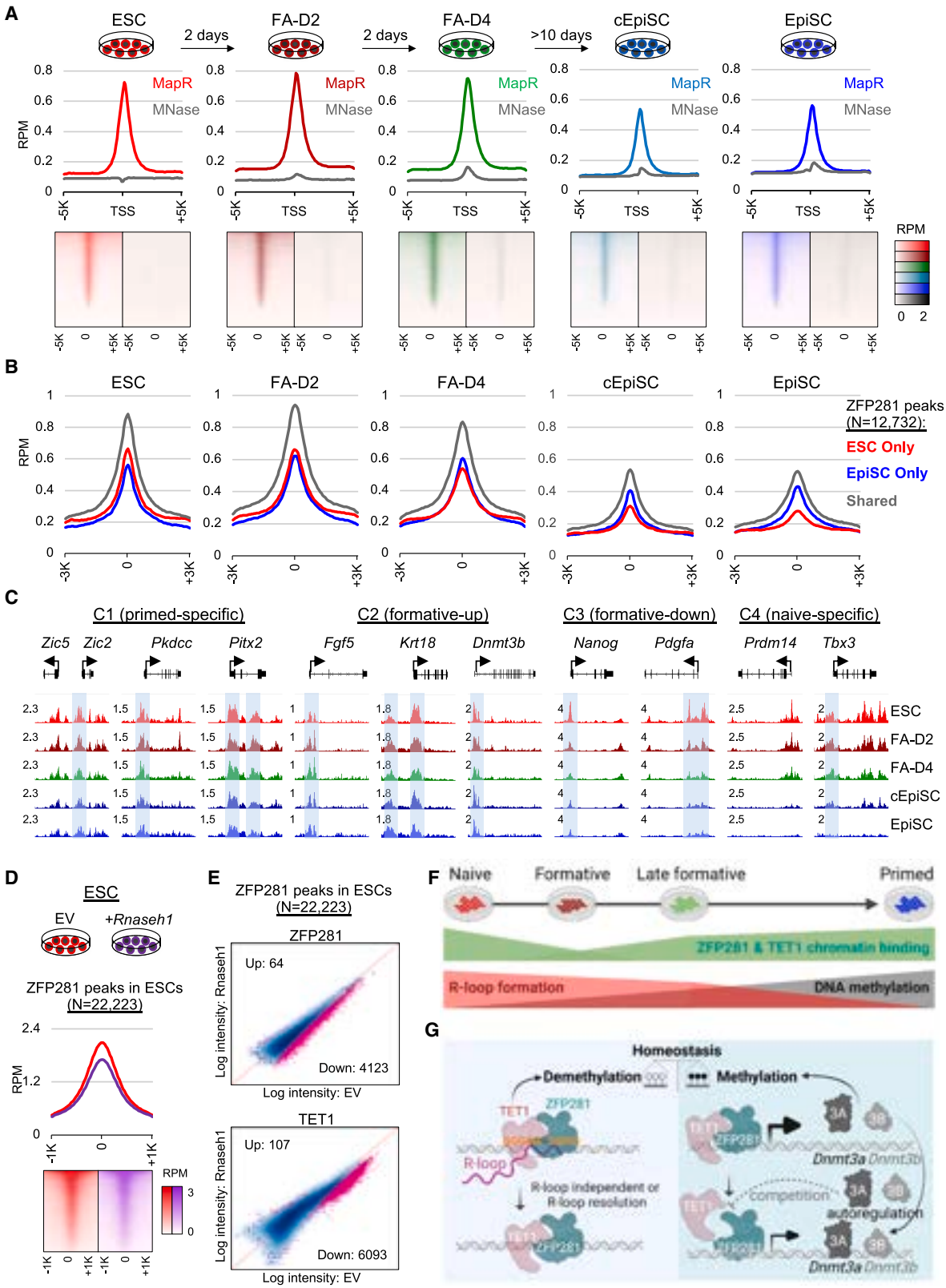

Figure 7. ZFP281 chromatin association depends on the formation of R-loops

(A) Schematic depiction of MapR analysis in ESC, FA-D2, FA-D4, cEpiSC, and EpiSC states (top), and mean intensity plots of MapR vs. control MNase signal at all TSSs (±5,000 bp). MapR was performed with biological replicates (n = 2).

(legend continued on next page)

methyltransferase EHMT1 and zinc finger TF ZIC2 were reported as two critical functional players acting downstream of ZFP281 both in driving exit from the ESC (naive) state and in restricting reprogramming of EpiSCs (primed) to an ESC state.[25] In addition, we have shown that ZFP281 activates *miR-302/367* to repress TET2 expression for establishing and maintaining primed pluripotency.[21] Of note, the defects observed in *Zfp281*KO embryos include failure of distal visceral endoderm/anterior visceral endoderm (DVE/AVE) specification, migration, and anterior-posterior (A-P) axis formation at E6.5,[22] which may or may not be directly linked to the DNA epigenetic regulation by ZFP281 identified in this study. The roles of ZFP281 in regulating DNMT3 and TET1 activities at gastrulation (E6.5–E8.5) are possible based on a single-cell RNA-seq dataset of mouse gastrulation (E6.5–E8.5),[45] which demonstrates that *Zfp281*, but not *Oct4* or *Nanog*, is broadly expressed together with *Dnmt3a/3b* and *Tet1* in the epiblast and in different lineage-specific precursors from E6.5 onward (Figures S7I and S7J). Therefore, we conclude that ZFP281 is an important TF orchestrating the transcription and DNA methylation landscapes during pluripotent state transitions and early embryonic development.

R-loops have long been considered an accidental by-product of transcription, although their roles in opening double-stranded DNA structures to maintain active transcription are also recognized.[46] Depletion of R-loops by overexpressing *Rnaseh1* in ESCs mildly impedes ESC differentiation.[47] We established R-loop dependent chromatin occupancy of ZFP281 and TET1 in ESCs (Figures 7D and 7E), which may partly explain the function of R-loops in ESC differentiation. In addition, R-loops formation is relatively stable at promoters of lineage-specific genes (Figures 7A–7C), although transcription of these R-loop-associated genes is repressed in ESCs. This observation aligns with prior findings that PRC2-repressed bivalent genes still maintain a low transcription activity in ESCs[35,48] and that PRC2 binding at promoters of developmental regulator genes depends on R-loops.[49] Because R-loop is also a threat to genome stability,[50] it was reported that the TET1/5hmC/R-loop-rich loci are prone to DNA damage in ESCs.[37] Interestingly, a recent study also suggests that ZFP281 is a critical factor for R-loop resolution through recruitment of BRCA2,[51] a DNA damage repair associated factor that can further recruit RNA helicase DDX5 to promote R-loop resolution.[52] Therefore, ZFP281 may have dual functions related to R-loops. On one hand, the formation of R-loops maintains ZFP281 and TET1 chromatin binding, on the other hand, ZFP281 employs the R-loop resolution mechanism to protect genome stability. Future studies are warranted to understand the functional interplay between R-loops and ZFP281 for genome stability during these critical cell state transitions.

Limitations of the study

Our study demonstrates that both DNMT3A and DNMT3B are transcriptionally activated by ZFP281 during pluripotent state transitions, although we cannot formally rule out that their protein levels could also be regulated by ZFP281 at additional levels (e.g., protein degradation). In addition, DNMT3A and DNMT3B are known to have unique functions in ESCs and early development.[28,34,53,54] Future studies are needed to distinguish the functions and targets of DNMT3A vs. DNMT3B (and possibly the isoforms associated with each gene) in different PSCs and during pluripotent state transitions. In addition, DNMT1 was reported to possess *de novo* DNA methylation activity in mouse oocytes,[55] but we can only speculate that DNMT1 may compensate for the loss of *de novo* DNA methylation activities in establishing *Dnmt3a/3b*-DKO cEpiSCs. Considering the dual catalytic and noncatalytic function of DNMT1,[56] it is also an open question whether the failure to derive cEpiSCs from *Dnmt1/3a/3b*-TKO but not *Dnmt3a/3b*-DKO is due to the lack of DNA-methylation-dependent and/or -independent functions.

STAR★METHODS

Detailed methods are provided in the online version of this paper and include the following:

- KEY RESOURCES TABLE
- RESOURCE AVAILABILITY
  - Lead contact
  - Materials availability
  - Data and code availability
- EXPERIMENTAL MODEL AND STUDY PARTICIPANT DETAILS
  - Cell culture and pluripotent state transition
  - Mouse study
  - *Zfp281*^{degron} knock-in (KI) and protein degradation
- METHOD DETAILS
  - Single-cell quantitative immunofluorescence (qIF)

(B) Mean intensity plot depicting the R-loop intensity at ESC-only, EpiSC-only, and ESC/EpiSC-shared ZFP281 peaks (from Figure 4B, ±3,000 bp).
(C) MapR tracks (numbers indicate RPM values) depicting the R-loop distribution at ZFP281-bound representative C1∼C4 genes. The shadows indicate ZFP281-bound promoters.
(D) Schematic depiction of ESCs with empty vector (EV) or *Rnaseh1* overexpression (top), mean intensity plots (middle) and intensity heatmaps (bottom) depicting ZFP281 ChIP intensity enriched at ZFP281 peaks (±1,000 bp). ChIP-seq was performed with biological replicates (n = 2).
(E) Scatterplots depicting the ZFP281 (top) and TET1 (bottom, from a published study[38]) ChIP intensity at ZFP281 peaks (N = 22,223) in ESCs with EV or *Rnaseh1* overexpression. Peaks with significantly different intensity is determined by $p < 0.05$.
(F and G) A model of ZFP281 functions in controlling transcription and DNA methylation landscapes in pluripotent state transitions.
(F) Depiction of the bimodal high-low-high pattern of ZFP281 and TET1 chromatin occupancy, decreased R-loop formation, and increased DNA methylation during the naive, formative, late formative, and primed transitions.
(G) Depiction of the interplay among ZFP281, TET1, and DNMT3A/3B for the DNA methylation/demethylation homeostasis during the pluripotent state transitions. Left: ZFP281-TET1 chromatin co-occupancy at ZFP281 target sites is dependent on R-loops. The presumed function of ZFP281 in R-loop resolution and potential R-loop-independent chromatin binding by ZFP281 and/or TET1 are also shown. Right: ZFP281 and TET1 transcriptionally activate *Dnmt3a* and *Dnmt3b* in E6.5 epiblast and different PSCs (ESCs, EpiLCs, and EpiSCs), whose translation products (DNMT3A and DNMT3B) bind to their own gene bodies for autoregulation. The potential competition between TET1 and DNMT3A/3B, reported previously in ESCs[13] and indicated with dashed inhibition lines, would lead to downregulation of ZFP281-regulated genes, including *Dnmt3a/3b* (and thus reduced 5mC levels), which in turn relieves TET1 from the competition, leading to heightened TET1 chromatin binding (and thus increased 5hmC levels).

- Small-scale TELP-enabled methylome sequencing (STEM-seq)
- *Rnaseh1* overexpression
- Western blot analysis
- DNA-RNA IP (DRIP) and methylation DNA-IP (meDIP) analysis
- Dot blot analysis
- Genomic DNA 5mC and 5hmC quantification by mass spectrometry
- Zfp281 shRNA knockdown
- RT-qPCR
- Chromatin immunoprecipitation (ChIP) and sequencing
- RNA sequencing
- MapR assay

- QUANTIFICATION AND STATISTICAL ANALYSIS
  - ChIP-seq and MapR data processing
  - RNA-seq data processing
  - Gene set enrichment analysis (GSEA) and gene ontology (GO) analysis
  - Single-cell analysis of mouse embryo tissues
  - Statistical analysis

SUPPLEMENTAL INFORMATION

Supplemental information can be found online at https://doi.org/10.1016/j.devcel.2023.12.018.

ACKNOWLEDGMENTS

We thank Dr. Taiping Chen for the DNMT KO ESCs, Dr. Guo-Liang Xu for the DNMT3A and DNMT3B antibodies for embryo staining, and Dr. Isao Suetake for providing the DNMT3L antibody for embryo staining. We thank Dr. Kavitha Sarma for providing the recombinant proteins for MapR assay. This work was supported by the National Institutes of Health (NIH) to X.H. (R21HD106263), B.C. (R01DK134610, R01HL167107), J.W. (R01GM129157, R01HD095938, R01HD097268, and R01HL146664), and A.-K.H. (R01DK127821, R01HD094868, and P30CA008748) and by contracts from New York State Stem Cell Science (NYSTEM) to J.W. (C35583GG and C35584GG).

AUTHOR CONTRIBUTIONS

X.H. conceived, designed, and conducted the study, performed bioinformatics analysis, and wrote the manuscript. S.B. and A.-K.H. performed embryo staining. C.L. and H.W. performed mass spectrometry analysis. Y.X., Y.Z., and W.X. performed STEM-seq of mouse embryos and data analysis. V.M., B.C., and H.Z. provided reagents and contributed to experiments. J.W. conceived the project, designed the experiments, and prepared and approved the manuscript.

DECLARATION OF INTERESTS

The authors declare no competing interests.

Received: April 3, 2023
Revised: November 4, 2023
Accepted: December 27, 2023
Published: January 17, 2024

REFERENCES

1. Zhang, Y., Xiang, Y., Yin, Q., Du, Z., Peng, X., Wang, Q., Fidalgo, M., Xia, W., Li, Y., Zhao, Z.A., et al. (2018). Dynamic epigenomic landscapes during early lineage specification in mouse embryos. Nat. Genet. *50*, 96–105.
2. Li, E., and Zhang, Y. (2014). DNA methylation in mammals. Cold Spring Harb. Perspect. Biol. *6*, a019133.
3. Smith, Z.D., and Meissner, A. (2013). DNA methylation: roles in mammalian development. Nat. Rev. Genet. *14*, 204–220.
4. Li, E., Bestor, T.H., and Jaenisch, R. (1992). Targeted mutation of the DNA methyltransferase gene results in embryonic lethality. Cell *69*, 915–926.
5. Okano, M., Bell, D.W., Haber, D.A., and Li, E. (1999). DNA methyltransferases Dnmt3a and Dnmt3b are essential for de novo methylation and mammalian development. Cell *99*, 247–257.
6. Gu, T., Hao, D., Woo, J., Huang, T.W., Guo, L., Lin, X., Guzman, A.G., Tovy, A., Rosas, C., Jeong, M., et al. (2022). The disordered N-terminal domain of DNMT3A recognizes H2AK119ub and is required for postnatal development. Nat. Genet. *54*, 625–636.
7. Kohli, R.M., and Zhang, Y. (2013). TET enzymes, TDG and the dynamics of DNA demethylation. Nature *502*, 472–479.
8. Dai, H.Q., Wang, B.A., Yang, L., Chen, J.J., Zhu, G.C., Sun, M.L., Ge, H., Wang, R., Chapman, D.L., Tang, F., et al. (2016). TET-mediated DNA demethylation controls gastrulation by regulating Lefty-Nodal signalling. Nature *538*, 528–532.
9. Charlton, J., Jung, E.J., Mattei, A.L., Bailly, N., Liao, J., Martin, E.J., Giesselmann, P., Brändl, B., Stamenova, E.K., Müller, F.J., et al. (2020). TETs compete with DNMT3 activity in pluripotent cells at thousands of methylated somatic enhancers. Nat. Genet. *52*, 819–827.
10. Wang, Q., Yu, G., Ming, X., Xia, W., Xu, X., Zhang, Y., Zhang, W., Li, Y., Huang, C., Xie, H., et al. (2020). Imprecise DNMT1 activity coupled with neighbor-guided correction enables robust yet flexible epigenetic inheritance. Nat. Genet. *52*, 828–839.
11. Neri, F., Rapelli, S., Krepelova, A., Incarnato, D., Parlato, C., Basile, G., Maldotti, M., Anselmi, F., and Oliviero, S. (2017). Intragenic DNA methylation prevents spurious transcription initiation. Nature *543*, 72–77.
12. Weinberg, D.N., Papillon-Cavanagh, S., Chen, H., Yue, Y., Chen, X., Rajagopalan, K.N., Horth, C., McGuire, J.T., Xu, X., Nikbakht, H., et al. (2019). The histone mark H3K36me2 recruits DNMT3A and shapes the intergenic DNA methylation landscape. Nature *573*, 281–286.
13. Gu, T., Lin, X., Cullen, S.M., Luo, M., Jeong, M., Estecio, M., Shen, J., Hardikar, S., Sun, D., Su, J., et al. (2018). DNMT3A and TET1 cooperate to regulate promoter epigenetic landscapes in mouse embryonic stem cells. Genome Biol. *19*, 88.
14. Wiehle, L., Raddatz, G., Musch, T., Dawlaty, M.M., Jaenisch, R., Lyko, F., and Breiling, A. (2016). Tet1 and Tet2 Protect DNA Methylation Canyons against Hypermethylation. Mol. Cell. Biol. *36*, 452–461.
15. Dixon, G., Pan, H., Yang, D., Rosen, B.P., Jashari, T., Verma, N., Pulecio, J., Caspi, I., Lee, K., Stransky, S., et al. (2021). QSER1 protects DNA methylation valleys from de novo methylation. Science *372*, eabd0875.
16. Wu, J., and Izpisua Belmonte, J.C. (2015). Dynamic pluripotent stem cell states and their applications. Cell Stem Cell *17*, 509–525.
17. Smith, A. (2017). Formative pluripotency: the executive phase in a developmental continuum. Development *144*, 365–373.
18. Loh, K.M., and Lim, B. (2011). A precarious balance: pluripotency factors as lineage specifiers. Cell Stem Cell *8*, 363–369.
19. Morgani, S., Nichols, J., and Hadjantonakis, A.K. (2017). The many faces of pluripotency: in vitro adaptations of a continuum of in vivo states. BMC Dev. Biol. *17*, 7.
20. Buecker, C., Srinivasan, R., Wu, Z., Calo, E., Acampora, D., Faial, T., Simeone, A., Tan, M., Swigut, T., and Wysocka, J. (2014). Reorganization of enhancer patterns in transition from naive to primed pluripotency. Cell Stem Cell *14*, 838–853.
21. Fidalgo, M., Huang, X., Guallar, D., Sanchez-Priego, C., Valdes, V.J., Saunders, A., Ding, J., Wu, W.S., Clavel, C., and Wang, J. (2016). Zfp281 coordinates opposing functions of Tet1 and Tet2 in pluripotent states. Cell Stem Cell *19*, 355–369.
22. Huang, X., Balmer, S., Yang, F., Fidalgo, M., Li, D., Guallar, D., Hadjantonakis, A.K., and Wang, J. (2017). Zfp281 is essential for mouse

epiblast maturation through transcriptional and epigenetic control of Nodal signaling. eLife *6*.

23. Zang, R., Huang, X., Li, D., Zhou, H., Gao, S., and Wang, J. (2022). Zfp281 is essential for epiblast maturation through a cell autonomous effect. J. Genet. Genomics *49*, 85–88.
24. Ying, Q.L., Wray, J., Nichols, J., Batlle-Morera, L., Doble, B., Woodgett, J., Cohen, P., and Smith, A. (2008). The ground state of embryonic stem cell self-renewal. Nature *453*, 519–523.
25. Mayer, D., Stadler, M.B., Rittirsch, M., Hess, D., Lukonin, I., Winzi, M., Smith, A., Buchholz, F., and Betschinger, J. (2020). Zfp281 orchestrates interconversion of pluripotent states by engaging Ehmt1 and Zic2. EMBO J. *39*, e102591.
26. Khoueiry, R., Sohni, A., Thienpont, B., Luo, X., Velde, J.V., Bartoccetti, M., Boeckx, B., Zwijsen, A., Rao, A., Lambrechts, D., and Koh, K.P. (2017). Lineage-specific functions of TET1 in the postimplantation mouse embryo. Nat. Genet. *49*, 1061–1072.
27. Ficz, G., Hore, T.A., Santos, F., Lee, H.J., Dean, W., Arand, J., Krueger, F., Oxley, D., Paul, Y.L., Walter, J., et al. (2013). FGF signaling inhibition in ESCs drives rapid genome-wide demethylation to the epigenetic ground state of pluripotency. Cell Stem Cell *13*, 351–359.
28. Auclair, G., Guibert, S., Bender, A., and Weber, M. (2014). Ontogeny of CpG island methylation and specificity of DNMT3 methyltransferases during embryonic development in the mouse. Genome Biol. *15*, 545.
29. Saiz, N., Kang, M., Schrode, N., Lou, X., and Hadjantonakis, A.K. (2016). Quantitative Analysis of Protein Expression to Study Lineage Specification in Mouse Preimplantation Embryos. J. Vis. Exp. 53654.
30. Nabet, B., Roberts, J.M., Buckley, D.L., Paulk, J., Dastjerdi, S., Yang, A., Leggett, A.L., Erb, M.A., Lawlor, M.A., Souza, A., et al. (2018). The dTAG system for immediate and target-specific protein degradation. Nat. Chem. Biol. *14*, 431–441.
31. Manzo, M., Wirz, J., Ambrosi, C., Villaseñor, R., Roschitzki, B., and Baubec, T. (2017). Isoform-specific localization of DNMT3A regulates DNA methylation fidelity at bivalent CpG islands. EMBO J. *36*, 3421–3434.
32. Sakaue, M., Ohta, H., Kumaki, Y., Oda, M., Sakaide, Y., Matsuoka, C., Yamagiwa, A., Niwa, H., Wakayama, T., and Okano, M. (2010). DNA methylation is dispensable for the growth and survival of the extraembryonic lineages. Curr. Biol. *20*, 1452–1457.
33. Adachi, K., Kopp, W., Wu, G., Heising, S., Greber, B., Stehling, M., Araúzo-Bravo, M.J., Boerno, S.T., Timmermann, B., Vingron, M., and Scholer, H.R. (2018). Esrrb unlocks silenced enhancers for reprogramming to naive pluripotency. Cell Stem Cell *23*, 900–904.
34. Baubec, T., Colombo, D.F., Wirbelauer, C., Schmidt, J., Burger, L., Krebs, A.R., Akalin, A., and Schübeler, D. (2015). Genomic profiling of DNA methyltransferases reveals a role for DNMT3B in genic methylation. Nature *520*, 243–247.
35. Huang, X., Bashkenova, N., Hong, Y., Lyu, C., Guallar, D., Hu, Z., Malik, V., Li, D., Wang, H., Shen, X., et al. (2022). A TET1-PSPC1-Neat1 molecular axis modulates PRC2 functions in controlling stem cell bivalency. Cell Rep. *39*, 110928.
36. Ginno, P.A., Lott, P.L., Christensen, H.C., Korf, I., and Chédin, F. (2012). R-loop formation is a distinctive characteristic of unmethylated human CpG island promoters. Mol. Cell *45*, 814–825.
37. Sabino, J.C., de Almeida, M.R., Abreu, P.L., Ferreira, A.M., Caldas, P., Domingues, M.M., Santos, N.C., Azzalin, C.M., Grosso, A.R., and de Almeida, S.F. (2022). Epigenetic reprogramming by TET enzymes impacts co-transcriptional R-loops. eLife *11*, e69476.
38. Arab, K., Karaulanov, E., Musheev, M., Trnka, P., Schäfer, A., Grummt, I., and Niehrs, C. (2019). GADD45A binds R-loops and recruits TET1 to CpG island promoters. Nat. Genet. *51*, 217–223.
39. Yan, Q., Shields, E.J., Bonasio, R., and Sarma, K. (2019). Mapping native R-loops genome-wide using a targeted nuclease approach. Cell Rep. *29*, 1369–1380.e5.
40. Wulfridge, P., and Sarma, K. (2021). A nuclease- and bisulfite-based strategy captures strand-specific R-loops genome-wide. eLife *10*, e65146.
41. Nichols, J., and Smith, A. (2009). Naive and primed pluripotent states. Cell Stem Cell *4*, 487–492.
42. Weinberger, L., Ayyash, M., Novershtern, N., and Hanna, J.H. (2016). Dynamic stem cell states: naive to primed pluripotency in rodents and humans. Nat. Rev. Mol. Cell Biol. *17*, 155–169.
43. Di Stefano, B., Ueda, M., Sabri, S., Brumbaugh, J., Huebner, A.J., Sahakyan, A., Clement, K., Clowers, K.J., Erickson, A.R., Shioda, K., et al. (2018). Reduced MEK inhibition preserves genomic stability in naive human embryonic stem cells. Nat. Methods *15*, 732–740.
44. Choi, J., Huebner, A.J., Clement, K., Walsh, R.M., Savol, A., Lin, K., Gu, H., Di Stefano, B., Brumbaugh, J., Kim, S.Y., et al. (2017). Prolonged Mek1/2 suppression impairs the developmental potential of embryonic stem cells. Nature *548*, 219–223.
45. Pijuan-Sala, B., Griffiths, J.A., Guibentif, C., Hiscock, T.W., Jawaid, W., Calero-Nieto, F.J., Mulas, C., Ibarra-Soria, X., Tyser, R.C.V., Ho, D.L.L., et al. (2019). A single-cell molecular map of mouse gastrulation and early organogenesis. Nature *566*, 490–495.
46. Niehrs, C., and Luke, B. (2020). Regulatory R-loops as facilitators of gene expression and genome stability. Nat. Rev. Mol. Cell Biol. *21*, 167–178.
47. Chen, P.B., Chen, H.V., Acharya, D., Rando, O.J., and Fazzio, T.G. (2015). R loops regulate promoter-proximal chromatin architecture and cellular differentiation. Nat. Struct. Mol. Biol. *22*, 999–1007.
48. Boyer, L.A., Plath, K., Zeitlinger, J., Brambrink, T., Medeiros, L.A., Lee, T.I., Levine, S.S., Wernig, M., Tajonar, A., Ray, M.K., et al. (2006). Polycomb complexes repress developmental regulators in murine embryonic stem cells. Nature *441*, 349–353.
49. Skourti-Stathaki, K., Torlai Triglia, E., Warburton, M., Voigt, P., Bird, A., and Pombo, A. (2019). R-loops enhance polycomb repression at a subset of developmental regulator genes. Mol. Cell *73*, 930–945.e4.
50. Skourti-Stathaki, K., and Proudfoot, N.J. (2014). A double-edged sword: R loops as threats to genome integrity and powerful regulators of gene expression. Genes Dev. *28*, 1384–1396.
51. Wang, Y., Ma, B., Liu, X., Gao, G., Che, Z., Fan, M., Meng, S., Zhao, X., Sugimura, R., Cao, H., et al. (2022). ZFP281-BRCA2 prevents R-loop accumulation during DNA replication. Nat. Commun. *13*, 3493.
52. Sessa, G., Gómez-González, B., Silva, S., Pérez-Calero, C., Beaurepere, R., Barroso, S., Martineau, S., Martin, C., Ehlén, Å., Martínez, J.S., et al. (2021). BRCA2 promotes DNA-RNA hybrid resolution by DDX5 helicase at DNA breaks to facilitate their repairdouble dagger. EMBO J. *40*, e106018.
53. Lauria, A., Meng, G., Proserpio, V., Rapelli, S., Maldotti, M., Polignano, I.L., Anselmi, F., Incarnato, D., Krepelova, A., Donna, D., et al. (2023). DNMT3B supports meso-endoderm differentiation from mouse embryonic stem cells. Nat. Commun. *14*, 367.
54. Mukamel, Z., Lifshitz, A., Mittnenzweig, M., Chomsky, E., Schwartzman, O., Ben-Kiki, O., Zerbib, M., and Tanay, A. (2022). DNA methyltransferases 3A and 3B target specific sequences during mouse gastrulation. Nat. Struct. Mol. Biol. *29*, 1252–1265.
55. Li, Y., Zhang, Z., Chen, J., Liu, W., Lai, W., Liu, B., Li, X., Liu, L., Xu, S., Dong, Q., et al. (2018). Stella safeguards the oocyte methylome by preventing de novo methylation mediated by DNMT1. Nature *564*, 136–140.
56. Mohan, K.N. (2022). DNMT1: catalytic and non-catalytic roles in different biological processes. Epigenomics *14*, 629–643.
57. Mohn, F., Weber, M., Schübeler, D., and Roloff, T.C. (2009). Methylated DNA immunoprecipitation (MeDIP). Methods Mol. Biol. *507*, 55–64.
58. Lai, W., Lyu, C., and Wang, H. (2018). Vertical ultrafiltration-facilitated DNA digestion for rapid and sensitive UHPLC-MS/MS detection of DNA modifications. Anal. Chem. *90*, 6859–6866.
59. Yan, Q., and Sarma, K. (2020). MapR: a method for identifying native R-loops genome wide. Curr. Protoc. Mol. Biol. *130*, e113.

STAR★METHODS

KEY RESOURCES TABLE

REAGENT or RESOURCE	SOURCE	IDENTIFIER
Antibodies		
ZFP281	Santa Cruz	Cat. sc-166933; RRID:AB_10612046
ZFP281	Abcam	Cat. ab101318; RRID: AB_11157929
DNMT1	Cell signaling	Cat. 5032S; RRID:AB_10548197
DNMT3A	Cell Signaling	Cat. 3598; RRID:AB_2277449
DNMT3A	R&D	Cat. MAB63151; RRID:AB_10972460
DNMT3B	R&D	Cat. NB300-516; RRID:AB_10003018
SUZ12	Abcam	Cat. ab12073; RRID: AB_442939
TET1	GeneTex	Cat. GTX125888; RRID: AB_11164485
TET2	Abcam	Cat. ab124297; RRID: AB_2722695
OCT4	Santa Cruz	Cat. sc-5279; RRID: AB_628051
NANOG	Bethyl	Cat. A300-397A; RRID: AB_386108
ESRRB	R&D	Cat. PP-H6707; RRID: AB_2100411
HA	Abcam	Cat. ab9110; RRID: AB_307019
KLF4	R&D	Cat. AF3640; RRID:AB_2130224
LEFTY	Santa Cruz	Cat. sc-365845; RRID:AB_10847353
RNASEH1	ProteinTech	Cat. 15606-1-AP; RRID:AB_2238624
ACTIN	Sigma	Cat. A5441; RRID: AB_476744
GAPDH	ProteinTech	Cat. 10494-1-AP; RRID: AB_2263076
VCL	Abcam	Cat. ab129002; RRID: AB_11144129
Rabbit IgG	Millipore	Cat. PP64; RRID: AB_97852
Mouse IgG	Millipore	Cat. 12-371; RRID:AB_145840
Mouse IgG HRP	Cell Signaling	Cat. 7076S; RRID: AB_330924
Rabbit IgG HRP	Jackson ImmunoRes	Cat. 715-175-151; RRID: AB_2340820
DNA 5mC	Cell Signaling	Cat. 28692; RRID: AB_2798962
DNA 5hmC	Active Motif	Cat. 39769; RRID: AB_10013602
DNA 5mC	Millipore	Cat. MABE146; RRID: AB_10863148
DNA-RNA hybrid S9.6	Millipore	Cat. MABE1095; RRID: AB_2861387
Chemicals, peptides, and recombinant proteins		
DMEM	GIBCO	Cat. 11965-092
Heat inactivated FBS	GIBCO	Cat. 35-011-CV
Penicillin-Streptomycin	GIBCO	Cat. 15140-122
L-Glutamine	GIBCO	Cat. 25030-081
MEM NEAA	GIBCO	Cat. 11140-050
2-Mercaptoethanol	Sigma	Cat. M6250
N2	GIBCO	Cat. 17502-048
B27	GIBCO	Cat. 17504-044
DMEM/F-12	GIBCO	Cat. 11-330-032
Neurobasal	GIBCO	Cat. 21-103-049
LIF	Lab prep	N/A
Recombinant Fgf2	R&D System	Cat. 233-FB
Recombinant Activin A	R&D System	Cat. 338-AC
dTAG-13	Tocris	Cat. 6605
Fibronectin	Millipore	Cat. FC010
Hygromycin	Omega	Cat. HG-80

(*Continued on next page*)

Continued

REAGENT or RESOURCE	SOURCE	IDENTIFIER
Puromycin	Sigma	Cat. P9620-10ML
Lipofectamine 3000	Invitrogen	Cat. L3000015
Deposited data		
Uncropped Western blot images	Mendeley Data	https://doi.org/10.17632/vp9wxrhf5k.1
TET1 ChIP-seq in PSCs	This paper	NCBI GEO: GSE226042
ZFP281 ChIP-seq in PSCs	This paper	NCBI GEO: GSE226042
HA ChIP-seq in *Zfp281*^{degron} PSCs	This paper	NCBI GEO: GSE226042
ZFP281 ChIP-seq in ESC with Rnaseh1 overexpression	This paper	NCBI GEO: GSE226042
DNMT3A/3B ChIP-seq in EpiSC	This paper	NCBI GEO: GSE226042
TET1 ChIP-seq in *Zfp281*^{degron} ESC and EpiSC	This paper	NCBI GEO: GSE226042
RNA-seq of *Zfp281*^{degron} PSCs with or without dTAG treatment	This paper	NCBI GEO: GSE226042
STEM-seq of WT, Zfp281$^{+/-}$, Zfp281$^{-/-}$ E6.5 embryos	This paper	NCBI GEO: GSE226042
MapR in PSCs	This paper	NCBI GEO: GSE226042
RNA-seq of WT PSCs (ESC, FA-D2, FA-D4)	Huang et al.[35]	NCBI GEO: GSE182443
RNA-seq of E3.5-E7.5 embryo tissues	Zhang et al.[1]	NCBI GEO: GSE76505
STEM-seq of E4.5-7.5 embryo tissues	Zhang et al.[1]	NCBI GEO: GSE76505
RNA-seq of WT and *Zfp281* mutant E6.5 embryos	Huang et al.[22]	NCBI GEO: GSE93044
DNMT3A/3B ChIP-seq in ESC	Baubec et al.[34]	NCBI GEO: GSE57413
OCT4, P300 ChIP-seq in ESC and EpiLC	Buecker et al.[20]	NCBI GEO: GSE56138
OCT4, NANOG ChIP-seq in EpiSC-to-ESC reprogramming	Adachi et al.[33]	ArrayExpress: E-MTAB-5342
TET1 ChIP-seq in ESC with Rnaseh1 overexpression	Arab et al.[38]	NCBI GEO: GSE104067
MapR in ESC	Wulfridge and Sarma[40]	NCBI GEO: GSE160578
Experimental models: Cell lines		
Mouse ESC J1, E14, and 3WT (CJ7 background)	This paper	N/A
Zfp281^{degron} ESC (J1 background) and cEpiSC	This paper	N/A
Mouse EpiSC OEC2, Episc9	This paper	N/A
WT, *Dnmt1*-KO, *Dnmt3a/3b*-DKO, and *Dnmt1/3a/3b*-TKO ESC	Laboratory of T. Chen	N/A
Oligonucleotides		
Oligonucleotides (see Table S3)	This paper	N/A
Software and algorithms		
STAR	2.7.6a	https://github.com/alexdobin/STAR
Cufflinks	2.2.1	http://cole-trapnell-lab.github.io/cufflinks/
Bowtie2	2.3.5	http://bowtie-bio.sourceforge.net/bowtie2/
IGV	2.10.2	https://software.broadinstitute.org/software/igv
BSseeker2	2.1.8	https://github.com/BSSeeker/BSseeker2
PICARD	2.18.5	https://broadinstitute.github.io/picard/
HOMER	4.11.1	http://homer.ucsd.edu/homer/
MACS2	2.2.7	https://github.com/macs3-project/MACS
Diffbind	3.2.7	https://bioconductor.org/packages/ release/ bioc/html/DiffBind.html
NGSplot	2.61	https://github.com/shenlab-sinai/ngsplot
GSEA	4.2.3	https://www.gsea-msigdb.org/gsea/

RESOURCE AVAILABILITY

Lead contact

Further information and requests for resources and reagents should be directed to and will be fulfilled by the lead contact, Jianlong Wang (jw3925@cumc.columbia.edu).

Materials availability

The *Zfp281*^{degron} ESCs generated in this paper are available from the lead contact with a completed Materials Transfer Agreement.

Data and code availability

The ChIP-seq, RNA-seq, STEM-seq, and MapR data have been deposited at Gene Expression Omnibus (GEO) with accession code: GSE226042. The deposited data are publicly available as of the date of publication. This paper analyzes existing, publicly available data. These accession numbers for the datasets are listed in the key resources table. Original uncropped Western blot images have been deposited to Mendeley Data and can be accessed using the following link: https://doi.org/10.17632/vp9wxrhf5k.1.

This paper does not report the original code.

Any additional information required to reanalyze the data reported in this paper is available from the lead contact upon request.

EXPERIMENTAL MODEL AND STUDY PARTICIPANT DETAILS

Cell culture and pluripotent state transition

Mouse ESCs were cultured on 0.1% gelatin-coated plates and in ES medium: DMEM medium supplemented with 15% fetal bovine serum (FBS), leukemia inhibitory factor (LIF, lab prepared), 0.1 mM 2-mercaptoethanol, 2 mM L-glutamine, 0.1 mM MEM non-essential amino acids (NEAA), 1% nucleoside mix (100X stock), and 50 U/mL Penicillin/Streptomycin (P/S). Mouse EpiSCs were cultured on fibronectin-coated (10 μg/mL) plates and in serum-free N2B27 medium supplemented with 0.1 mM 2-mercaptoethanol, 2 mM L-glutamine, 0.1 mM NEAA, 50 U/mL P/S, and supplemented with fresh Fgf2 (12 ng/mL) and Activin A (20 ng/mL) (FA medium). ESCs were passed with 0.05% Trypsin/EDTA, and EpiSCs were passed with Accutase. For proteasome inhibition, ESCs were treated with MG132 (5 μM, Sigma, M7449) for 6 hours.

For ESC-EpiLC-EpiSC differentiation, ESCs were seeded on fibronectin-coated (10 μg/mL) plates in ES medium overnight and switched to FA medium the next day. The adapted cells in FA medium for 2 days (FA-D2) and 4 days (FA-D4) were collected. After more than two weeks of FA culture, adapted cells were considered converted EpiSCs (cEpiSCs).

Mouse study

The *Zfp281*KO mice[22] were used in this study. All mice experiments were conducted in accordance with the guidelines approved by the Institutional Animal Care and Use Committee (IACUC) at Columbia University Irving Medical Center (PI: Jianlong Wang, protocol #AABD5612) and Memorial Sloan Kettering Cancer Center (PI: Hadjantonakis, protocol #03-12-017).

Zfp281^{degron} knock-in (KI) and protein degradation

The CRISPR/Cas9 system was used to engineer ESCs for protein degradation of ZFP281, as previously described.[35] The 5′- and 3′-homology arms of *Zfp281* for C-terminal insertion were PCR amplified from genomic DNA. The 5′- and 3′-homology arms and FKBP12^{F36V}-2xHA-mCherry fragment were assembled by Gibson Assembly 2x Master Mix (NEB, E2611S). The CRISPR gRNA was subcloned into the pSpCas9(BB)-2A-Puro (PX459) vector (gRNA sequence in Table S3). ESCs were transfected with the donor and CRISPR vectors using Lipofectamine 3000 (Invitrogen). After 2 days of puromycin selection, mCherry-positive cells were seeded on a 96-well plate with a single cell per well using the BD Influx Cell Sorter. Cells were expanded and genotyped by PCR. Two clones (#2 and #21) with a homozygous knock-in were further expanded and used for experiments. *Zfp281*^{degron} ESCs and cEpiSCs were treated with dTAG13 (500 nM in DMSO, Tocris, 6605) for degradation of ZFP281 protein.

METHOD DETAILS

Single-cell quantitative immunofluorescence (qIF)

E6.5 embryos were collected, and qIF was performed as we previously described. Briefly, embryos were permeabilized in PBS-0.5% Triton for 20 min at room temperature, washed in PBS-0.1% Triton (PBT), and blocked at 4°C o/n in PBT-3% BSA. Primary and secondary antibody staining was performed overnight at 4°C. Counterstaining with Hoechst and fluorophore-coupled phalloidin (Life Technologies, Carlsbad, CA) was performed for 1 h at room temperature, and images were taken on a Zeiss LSM880 laser scanning confocal microscope. Fluorescence intensity levels were measured on data acquired with the same imaging parameters. Postimplantation nuclear protein levels were quantified using Imaris software (Bitplane) by manually creating individual nuclear surfaces for each cell and quantifying the fluorescence level inside the volume defined by these surfaces. Statistical significance was calculated on the average level of corrected fluorescence per embryo using an unpaired two-tailed Student T-test with Welch's correction when standard deviations differed between samples. The following primary antibodies were used: ZFP281 (Santa Cruz, sc-166933), DNMT3A and DNMT3B (gift from Dr. Guo-Liang Xu), and DNMT3L (gift from Dr. Isao Suetake).

Small-scale TELP-enabled methylome sequencing (STEM-seq)

STEM-seq for low-input genome-wide DNA methylation profiling in epiblast cells of WT, *Zfp281*$^{+/-}$, and *Zfp281*$^{-/-}$ E6.5 embryos was performed as previously described.[1] All STEM-seq datasets were mapped to the mm9 genome by BSSeeker2. Alignments were performed with the following parameters in addition to the default parameters: –bt2-p 8 –XS 0.2,3 –a CCCCCC –m 4. Multi-mapped reads and PCR duplicates were removed. After validating the reproducibility between replicates, we pooled data from replicates for subsequent analyses. For methylation analysis, the CG methylation was calculated as the total methylated counts (combining Watson and Crick strands) divided by the total counts across all reads covering that CG.

Rnaseh1 overexpression

Mouse *Rnaseh1* coding sequence (CDS) was amplified from the cDNA of mouse ESCs by reverse transcription with SuperScript III Reverse Transcriptase (Invitrogen). Then, *Rnaseh1* CDS was cloned into a piggyBac (PB) expression vector with Hygromycin. The PB-*Rnaseh1*-Hygro and empty PB-Hygro vectors were cotransfected with helper PBase (encodes the transposase) vector in ESCs with Lipofectamine 3000 (Invitrogen). Transfected ESCs were selected with 100 μg/ml Hygromycin for one week with at least two passages.

Western blot analysis

For Western blot analysis, total proteins were extracted by RIPA buffer with a protease inhibitor cocktail (Sigma). Protein concentrations were measured by Bradford assay (Pierce, 23236), balanced, and subjected to SDS-PAGE analysis. The following primary antibodies were used: ZFP281 (Santa Cruz, sc-166933 and Abcam, ab101318), TET1 (GeneTex, GTX125888), DNMT1 (Cell signaling, 5032S), DNMT3A (R&D, MAB63151), DNMT3B (R&D, NB300-516), OCT4 (Santa Cruz, sc-5279), ESRRB (R&D, PP-H6707), KLF4 (R&D, AF3640), NANOG (Bethyl, A300-397A), RNASEH1 (ProteinTech, 15606-1-AP), TET2 (Abcam, ab124297), SUZ12 (Abcam, ab12073), LEFTY (Santa Cruz, sc-365845), ACTIN (Sigma, A5441), GAPDH (ProteinTech, 10494-1-AP), and Vinculin (VCL, Abcam, ab129002).

DNA-RNA IP (DRIP) and methylation DNA-IP (meDIP) analysis

The DRIP and meDIP followed by qPCR analysis were performed following the meDIP protocol[57] and a prior publication[47] with modifications. Briefly, ESCs were lysed in TE buffer with 0.05% SDS, 0.1 mg/mL proteinase K, and incubated at 37°C overnight with rotation. DNA was extracted using Phenol/Chloroform/Isoamylalcohol (Invitrogen, 15593-049), precipitated, and washed with 70% ethanol. Genomic DNA was resuspended in TE buffer and sonicated with Bioruptor Pico (settings of 30 sec ON, 30 sec OFF, 10 cycles).

For meDIP, the genomic DNA was treated with 20 μg/mL RNase A and incubated at 37°C for 30 min before sonication. After sonication, DNA was precipitated again and resuspended in TE buffer. For each DIP, 5 μg DNA was resuspended in 450 μL TE buffer and boiled at 95°C for 10 min, then immediately on ice, and 50 μL 10X MeDIP buffer was added. After mixing, 10 μL of DNA was used as Input. 3 μg 5mC (Millipore, MABE146), 5hmC (Active Motif, 39769), and mouse IgG (Millipore, 12-371) were added in each DIP. Samples were incubated overnight at 4°C with gentle rotation. Next day, samples were incubated with Protein G dynabeads (Invitrogen, 10004D) at 4°C for 2 h, and washed 4X with MeDIP buffer. The DNA was eluted and purified with NucleoSpin PCR Clean-up columns and NTB buffer (Macherey-Nagel, #740609 and #740595).

For each DRIP, 5 μg DNA resuspended in 500 μL MeDIP buffer and incubated with 3 μg DNA-RNA hybrid S9.6 antibody (Millipore, MABE1095) or mouse IgG (Millipore, 12-371). The other steps were the same as the meDIP analysis. DRIP- and meDIP-qPCR were performed with a QuantStudio 5 Real-Time PCR machine (Applied Biosystems). Percentages of input recovery were calculated. The DRIP- and meDIP-qPCR primers are listed in Table S3.

Dot blot analysis

The genomic DNA dot-blot analysis of 5mC and 5hmC was performed following the DNA Dot Blot Protocol (Cell Signaling, #28692), as previously described.[35] Briefly, genomic DNA was extracted using Quick-DNA Miniprep Plus Kit (Zymo Research, D4068), and DNA concentration was measured by NanoDrop. The same amount of DNA was denatured with 10X DNA denaturing buffer (1 M NaOH and 0.1 M EDTA) and incubated at 95°C for 10 min, which was then immediately mixed with an equal volume of 20X SSC buffer, pH 7.0 (Invitrogen, 15557044) and chilled on ice. The DNA samples were diluted with a pre-determined amount and loaded on the positive-charged Nylon membrane (GE Amersham, RPN2020B) using a vacuum chamber (Manifold, SRC-96). The membrane was dried, auto-crosslinked with 1200 x100 μJ/cm^2, and blocked with 5% milk/TBST for 1 h. Next, the membrane was incubated with 5mC (Cell Signaling, 28692) or 5hmC (Active Motif, 39769) antibodies, the same as the western blot analysis.

The DNA-RNA hybrid dot blot analysis was performed using the DRIP samples after sonication. Briefly, DNA samples were incubated with and without RNase H (NEB, 0297L) at 37°C for 6 h with rotation. After RNase H digestion, DNA was precipitated again and resuspended in TE buffer. Similarly, the DNA samples were diluted with a pre-determined amount and loaded on the positive-charged Nylon membrane (GE Amersham, RPN2020B) using a vacuum chamber (Manifold, SRC-96). The membrane was dried, auto-crosslinked with 1200 x100 μJ/cm2, and blocked with 5% milk/TBST for 1 h. Next, the membrane was incubated with S9.6 antibody (Millipore, MABE1095), the same as the western blot analysis.

Genomic DNA 5mC and 5hmC quantification by mass spectrometry

The UHPLC-MS/MS analysis for 5mC and 5hmC quantification was performed as previously described[58] on an Agilent 1290 Infinity II ultrahigh performance LC system coupled with an Agilent 6470 triple quadrupole mass spectrometer equipped with a jet stream electrospray ionization source (Santa Clara, CA). MS was operated under positive ionization using multiple reactions monitoring (MRM) mode: *m/z* 242->83 for 5mC and *m/z* 258->142 for 5hmC. The frequencies of 5mC and 5hmC over total deoxycytidine (dC) were calibrated by corresponding stable isotope-labeled internal standards.

Zfp281 shRNA knockdown

Zfp281 knockdown in ESCs and EpiSCs was performed as previously described,[21] with either a control empty vector or two independent *Zfp281* shRNAs.

RT-qPCR

Total RNA was extracted using the GeneJet RNA Purification Kit (Thermo Scientific, K0732). Reverse transcription was performed using the qScript kit (Quantabio, 95048). Relative expression levels were determined using a QuantStudio 5 Real-Time PCR System (Applied Biosystems). Gene expression levels were normalized to *Gapdh*. Primers for RT-qPCR are listed in Table S3.

Chromatin immunoprecipitation (ChIP) and sequencing

ChIP was performed as previously described.[35] Briefly, cell pellets were crosslinked with 1% (w/v) formaldehyde for 10 min at RT, followed by the addition of 125 mM glycine to stop the reaction. Next, chromatin extracts were sonicated into 200–500 bp with Bioruptor Plus (settings of 30 sec ON, 30 sec OFF, 30 cycles) or with Bioruptor Pico (settings of 30 sec ON, 30 sec OFF, 15 cycles). ChIP was performed with the following primary antibodies: ZFP281 (Abcam, ab101318), HA (Abcam, ab9110), TET1 (GenTex, GTX125888), DNMT3A (Cell Signaling, 3598), DNMT3B (R&D, NB300-516), or rabbit IgG (Millipore, PP64) overnight at 4°C with continuous mixing, followed by incubation with Protein G dynabeads (Invitrogen, 10004D) for 2 h at 4°C. The immunoprecipitated DNA was washed with ChIP RIPA buffer and purified with NucleoSpin PCR Clean-up columns and NTB buffer (Macherey-Nagel, #740609 and #740595). ChIP-qPCR was performed with a QuantStudio 5 Real-Time PCR machine (Applied Biosystems). Percentages of input recovery were calculated. The ChIP-qPCR primers are listed in Table S3.

For ChIP-seq, 10% of sonicated genomic DNA was used as ChIP input. Libraries were prepared using the NEBNext Ultra II DNA library prep kit and index primers sets (NEB, 7645S, E7335S) following the standard protocol. Sequencing was performed with the Illumina HiSeq 4000 Sequencer according to the manufacturer's protocol. Libraries were sequenced as 150-bp paired-end reads.

RNA sequencing

Total RNA was extracted using the GeneJet RNA Purification Kit (Thermo Scientific, K0732). RNA-seq library construction was performed at Novogene with a standard polyA-enrichment protocol. Sequencing was performed on an Illumina HiSeq 4000 Sequencer, and 150-bp paired-end reads were obtained.

MapR assay

MapR assay was performed following the MapR protocol[59] and using reagents in a CUT&Run (EpiCypher) setting. Briefly, one million cells were incubated with 10 μL Magnetic Concanavalin A Beads for 30 min with a gentle mix at room temperature. Then, the beads/cells were washed with wash buffer and resuspended in 50 μL digitonin buffer containing 0.02% digitonin. The GST-RHΔ-MNase or control GST-MNase recombinant proteins were added to a final protein concentration of 1 μM and incubated overnight at 4 °C with rotation. Next day, beads/cells were further washed with digitonin buffer and activated with 2 mM $CaCl_2$ for 30 min on ice. A 2X stop buffer was added to stop the MNase activity immediately. 5 μL spike-in DNA (*S. cerevisiae*, 10 pg/uL, Cell signaling, #40366) was added, and the rest of the protocol followed a standard CUT&Run (EpiCypher) procedure. About 100 ng MapR and 50 ng MNase DNA were used for libraries using the NEBNext Ultra II DNA library prep kit and index primers sets (NEB, 7645S, E7335S) following the standard protocol.

QUANTIFICATION AND STATISTICAL ANALYSIS

ChIP-seq and MapR data processing

All ChIP-seq and MapR reads were pre-processed by trim_galore (v0.6.3) and aligned to the mm9 mouse genome using the bowtie2 (v2.3.4) program and the parameters were "-X 1000 –no-mixed –no-discordant". The aligned reads were exported (-F 0x04 -f 0x02) and sorted with samtools. Duplicates were removed with MarkDuplicates function in the PICARD (v2.14.0) package. The aligned ChIP-seq bam files of ZFP281 ChIP in WT PSCs and HA-ChIP in *Zfp281*^{degron} PSCs were combined. Biological replicates of MapR data were also combined. All bam files were converted to a binary tiled file (tdf) and visualized using IGV (v2.7.2) software.

ChIP-seq peaks were determined by the MACS2 program (v.2.2.7), using the input ChIP-seq as the control data, and all other parameters were the default settings. The peak lists were filtered with a minimal score of >5. ChIP-seq peaks were annotated using the annotatePeaks module in the HOMER program (v4.11) against the mm9 genome. Motif analysis was performed using the findMotifsGenome module in HOMER, with parameters: -size given -len 10. A target gene of a called peak was defined as the nearest gene's transcription start site (TSS) with a distance to TSS less than 5 kb. Heatmaps and mean intensity curves of ChIP-seq data at specific

genomic regions were plotted by the NGSplot program (v2.61) centered by the middle point "(start+end)/2" of each region. Diffbind (v3.2.7) was used to compare the intensity of reads at specific regions between different ChIP-seq data. Peaks with significantly different depicting are determined by P<0.05.

RNA-seq data processing

For RNA-seq data processing, reads were aligned to the mouse genome mm9 using STAR (v2.7.6a) with the default settings. Transcript assembly and differential expression analyses were performed using Cufflinks (v2.2.1). Assembly of novel transcripts was not allowed (-G). Other parameters of Cufflinks were the default setting. The summed FPKM (fragments per kilobase per million mapped reads) of transcripts sharing each gene_id was calculated and exported by the Cuffdiff program. Differentially expressed genes (DEGs) were determined by two-sided T-test P-value<0.05 and fold-change>2 or by Q-value (FDR) < 0.05. Volcano plots for gene expression by fold change versus P-value were generated using R.

For hierarchical clustering analysis, the gene expression table was imported by Cluster 3.0 software. Mean-center and normalization of gene expression were performed, then the analysis was performed with the average-linkage of genes. Clustered genes with normalized expression values (z-score) were shown in Heatmap with the Java TreeView (v1.1.6) program.

For principal component analysis (PCA), batch effects were adjusted by the *ComBat* function implemented in the *sva* Bioconductor package (v.3.18.0). PCA was performed with the Cluster 3.0 software. PC values were visualized with the plot3d function in the rgl package using R (v4.1.0) scripts.

Gene set enrichment analysis (GSEA) and gene ontology (GO) analysis

GSEA (v4.2.3) was used to determine the statistically enriched gene sets by comparing the WT and untreated *Zfp281*^{degron} EpiSCs (Ctrl: 4 samples) and the 2 days and 4 days of dTAG-treated *Zfp281*^{degron} EpiSCs (dTAG: 4 samples). The curated C5: ontology gene sets were downloaded from https://www.gsea-msigdb.org/gsea/. GSEA enrichment plot, normalized enrichment score (NES), and Q-value (FDR) were indicated for each enrichment test.

Gene ontology (GO) analyses were performed using the DAVID gene ontology functional annotation tool (https://david.ncifcrf.gov/tools.jsp) with all *Mus musculus* genes as a reference list.

Single-cell analysis of mouse embryo tissues

The scRNA-seq data[45] with detailed annotation of gastrulating mouse embryo tissues (E6.5-E8.5) were available at https://marionilab.cruk.cam.ac.uk/MouseGastrulation2018/. Expression maps of gene-of-interest were downloaded by projection type: UMAP; cell subset: all timepoints; plot color: cell type.

Statistical analysis

If not specified, qPCR analysis was performed in technical triplicates. Histograms were generated using the GraphPad Prism software (v9.2.0), and the error bar indicates a standard deviation. The line plots in Figures 1C and 1D represent the mean expression value of each cluster with a 95% confidence interval (CI) using the GraphPad Prism software (v9.2.0). The boxplots in Figures 3F and 6F present the 25th, median, and 75th quartiles, and the whiskers extend 1.5 of interquartile ranges. The P-value was calculated from a paired two-sided Mann-Whitney test using R. The scatter plots in Figure S6B calculated the $\log_2$ ratio of gene expression (D4/D0 vs. D2/D0), and a linear regression line and coefficient of determination (R^2) value were calculated by Excel software. If not specified, statistical analysis was performed with R (v4.1.0) scripts on the R-Studio platform (v1.4.1). The statistical details of the experiment are indicated in the figure legend.